Published in : Computer methods in applied mechanics and engineering (2008), vol. 197, pp. 1184-1203
DOI: doi:10.1016/j.cma.2007.10.008
Status : Postprint (Author's version)

A SMOOTHED FINITE ELEMENT METHOD FOR PLATE ANALYSIS

H. Nguyen-Xuan [a], T. Rabczuk[b], Stephane Bordas[c]*, J.F. Debongnie[d]

[a] *Division of Computational Mechanics, Department of Mathematics and Informatics, University of Natural Sciences, VNU-HCM, 227 Nguyen Van Cu, Viet Nam*
[b] *Department of Mechanical Engineering, University of Canterbury, Private Bag 4800, Christchurch 8140, New Zealand*
[c] *University of Glasgow, Civil Engineering, Rankine building, G12 8LT, United Kingdom*
[d] *Division of Manufacturing, University of Liege, Batiment B52/3 Chemin des Chevreuils 1, B-4000 Liege 1, Belgium*

KEYWORDS: Plates; Curvature smoothing; Smooth finite element method; SFEM; Locking-free; Distorted meshes

ABSTRACT

A quadrilateral element with smoothed curvatures for Mindlin-Reissner plates is proposed. The curvature at each point is obtained by a non-local approximation via a smoothing function. The bending stiffness matrix is calculated by a boundary integral along the boundaries of the smoothing elements (smoothing cells). Numerical results show that the proposed element is robust, computational inexpensive and simultaneously very accurate and free of locking, even for very thin plates. The most promising feature of our elements is their insensitivity to mesh distortion.

Published in : Computer methods in applied mechanics and engineering (2008), vol. 197, pp. 1184-1203
DOI: doi:10.1016/j.cma.2007.10.008
Status : Postprint (Author's version)

1. Introduction

Plate structures play an important role in Engineering Science. There are two different plate theories, the Kirchhoff plate and the Mindlin-Reissner plate theory. Kirchhoff plates are only applicable for thin structures where shear stresses in the plate can be ignored. Moreover, Kirchhoff plate elements require C^1 continuous shape functions. Mindlin-Reissner plates take shear effects into account. An advantage of the Mindlin-Reissner model over the biharmonic plate model is that the energy involves only first derivatives of the unknowns and so conforming finite element approximations require only the use of C^0 shape functions instead of the required C^1 shape functions for the biharmonic model. However, Mindlin-Reissner plate elements exhibit a phenomenon called shear locking when the thickness of the plate tends to zero. Shear locking is characterized by incorrect transverse forces under bending. When linear finite element shape functions are used, the shear angle is linear within an element while the contribution of the displacement is only constant. The linear contribution of the rotation cannot be ''balanced" by a contribution from the displacement. Hence, the Kirchhoff constraint $w_{,x} + \beta_y = 0$, $w_{,y} + \beta x = 0$ is not fulfilled in the entire element any more. Typically, when shear locking occurs, there are large oscillating shear/transverse forces and hence a simple smoothing procedure can drastically improve the results. Early methods tried to overcome the shear locking phenomenon by reduced integration or a selective reduced integration, see Refs. [29,30,67]. The idea is to split the strain energy into two parts, one due to bending and the other one due to shear. Commonly, different integration rules for the bending strain and the shear strain energy are used. For example, for the shear strain energy, reduced integration is used while full integration is used for the bending energy. Reduced integration leads to an instability due to rank deficiency and results in zero-energy modes that can be eliminated by an hourglass control, [3,6,28,66].

For a general quadrilateral plate element, the deflection and the two rotations of the four-node element can be interpolated. Often, approximated fields of high degree are used. However, except for the 16-node isoparametric element of [66], most other elements still exhibit shear locking when the thickness tends to zero. To overcome this phenomenon, a reduced integration scheme is employed in the shear term. However, most of these elements still exhibit either locking or exhibit artificial zero-energy modes. Another famous class of plate elements are mixed formulation/hybrid elements [36,37,48] and equilibrium elements [25]. However, such elements are complex and the computational cost is high. They are not popular in most commercial finite element method (FEM) codes.

The assumed natural strain (ANS) method was developed to eliminate shear locking for bilinear plate elements, [31]. The basic idea is to compute the shear strains not directly from the derivatives of the displacements but at discrete collocation points, from the displacements. Afterwards, they are interpolated over the element with specific shape functions. For the bilinear element for example, the collocation points will be placed at the midpoint of the element edges since the shear stresses are linear in the element and zero in the middle of the element. This reduces in addition one of the constraints, since it makes one of the Kirchhoff constraints linear dependent on the other

Published in : Computer methods in applied mechanics and engineering (2008), vol. 197, pp. 1184-1203
DOI: doi:10.1016/j.cma.2007.10.008
Status : Postprint (Author's version)

constraints. Bathe and Dvorkin [4] extended the ANS plate elements to shells. The resulting element is known as the MITC (mixed interpolation of tensorial components) or Bathe-Dvorkin element, see also [5,24]. Many ANS versions of plate and shell elements have been developed. A nice overview can be found, e.g. in the textbooks by [66] and [3], as well as [49].

An alternative to the ANS method to avoid shear locking is the discrete-shear-gap (DSG) method [10]. The DSG method is in a way similar to the ANS method since it modifies the course of certain strains within the element. The main difference is the lack of collocation points that makes the DSG method independent of the order and form of the element. Instead, the Kirchhoff constraints are imposed directly on the element nodes. The enhanced- assumed-strain (EAS) method principally can be used to avoid locking phenomena as well. While the EAS method was successfully applied to eliminate membrane locking in shells, it was not very efficient in removing shear locking in plates. The EAS element of Simo and Rifai [53] gives satisfying results for rectangular plates.

In this work, we present new plate elements based on the MITC4 element in which we incorporate stabilized conforming nodal integration (SCNI). The SCNI approach was originally developed in meshfree methods as a normalization for nodal integration [17,64] of the meshfree Galerkin weak form and recently in the FEM [40]. In this approach, the strain smoothing stabilization has been introduced. In the SCNI, to meet the integration constraints and thus fulfills the linear exactness in the Galerkin approximation of the second order partial differential equations. Wang et al. [56] have shown that the cause of shear locking in Mindlin-Reissner plate formulations is due to the inability of the approximation functions to reproduce the Kirchhoff mode, and the incapability of the numerical method to achieve pure bending exactness (BE) in the Galerkin approximation. In their study, the Kirchhoff mode reproducing condition (KMRC) is ensured for Mindlin-Reissner plates. The approximation functions for the displacement and the rotations are constructed to meet the KMRC. Then, they derived the integration constraints for achieving BE, and a curvature smoothing method (CSM) is proposed to meet the bending integration constraints. A further extension of the SCNI to analysis of transverse and inplane loading of laminated anisotropic plates with general planar geometry was studied in [57]. Other contributions to remove shear locking in meshfree plate discretizations are given in [26,34,35,39,54], and, very recently, [2,19,57].

In meshfree methods with stabilized nodal integration, the entire domain is discretized into cells defined by the field of nodes, such as the cells of a Voronoi diagram [17,64]. Integration is performed along the edges of each cell. Although meshfree methods such as EFG obtain good accuracy and high convergence rates, the non-polynomial or usually complex approximation space increases the computational cost of numerical integration. Recently, applications of the SCNI to the FEM so-called the smoothed finite element method (SFEM) for two dimensional problems had been proposed by Liu et al. [40,41]. It was shown that the SFEM is stable, accurate and effective [20,21,47]. Following the idea of the SFEM, Nguyen et al. [46] have formulated the SFEM with a selective cell-wise smoothing technique in order to eliminate locking in incompressible cases, which have also been studied in [47].

We will show by numerical experiments that our element performs better or slightly better than the original MITC4 element, at least for all examples tested. Moreover, due to the integration technique,

Published in : Computer methods in applied mechanics and engineering (2008), vol. 197, pp. 1184-1203
DOI: doi:10.1016/j.cma.2007.10.008
Status : Postprint (Author's version)

the element promises to be more accurate especially for distorted meshes. We will also show that our element is free of shear locking.

The outline of the paper is organized as follows. In the next section, we present the basic equations of the plate problem and the weak form. The curvature smoothing stabilization and the finite element discretization using the curvature smoothing method are introduced in Section 3. Several numerical examples are given in Section 4. Finally, Section 5 closes this manuscript with some conclusions and future plans.

2. Governing equations and weak form

Let Ω be the domain in R^2 occupied by the mid-plane of the plate and w and $\beta = (\beta_x, \beta_y)^T$ denote the transverse displacement and the rotations in the $x - z$ and $y - z$ planes, see Fig. 1, respectively. Assuming that the material is homogeneous and isotropic with Young's modulus E and Poisson's ratio ν, the governing differential equations of the Mindlin-Reissner plate are

$$-\operatorname{div}\mathbf{D}^{\mathrm{b}}\boldsymbol{\kappa}(\boldsymbol{\beta}) - \lambda t\boldsymbol{\gamma}(\boldsymbol{\beta}) = 0 \quad \text{in } \Omega, \tag{1}$$

$$-\lambda t \operatorname{div}(\boldsymbol{\gamma}) = p \quad \text{in } \Omega, \tag{2}$$

$$w = \bar{w}, \quad \boldsymbol{\beta} = \bar{\boldsymbol{\beta}} \quad \text{on } \Gamma = \partial\Omega, \tag{3}$$

where t is the plate thickness, $p = p(x, y)$ is the transverse loading per unit area, $\lambda = \frac{kE}{2(1+\nu)}$, $k = 5/6$ is the shear correction factor and $\mathbf{D}^{\mathrm{b}}$ is the tensor of bending moduli, κ and γ are the bending and shear strains, respectively, defined as

$$\boldsymbol{\kappa} = \begin{bmatrix} \frac{\partial \beta_x}{\partial x} \\ -\frac{\partial \beta_y}{\partial y} \\ \frac{\partial \beta_x}{\partial y} - \frac{\partial \beta_y}{\partial x} \end{bmatrix}, \quad \boldsymbol{\gamma} = \begin{bmatrix} \frac{\partial w}{\partial x} + \beta_x \\ \frac{\partial w}{\partial y} - \beta_y \end{bmatrix}. \tag{4}$$

The Eqs. (1)-(3) correspond to the minimization of the total potential function

$$\Pi_{\mathrm{TPE}} = \frac{1}{2}\int_{\Omega} \boldsymbol{\kappa} : \mathbf{D}^{\mathrm{b}} : \boldsymbol{\kappa}\, \mathrm{d}\Omega + \frac{1}{2}\int_{\Omega} \boldsymbol{\gamma} : \mathbf{D}^{s} : \boldsymbol{\gamma}\, \mathrm{d}\boldsymbol{\Omega} - \int_{\Omega} wp\, \mathrm{d}\Omega. \tag{5}$$

The weak form of the equilibrium equation follows from the stationarity of Eq. (5):

$$\delta\Pi_{\mathrm{TPE}} = \int_{\Omega} \delta\boldsymbol{\kappa} : \mathbf{D}^{\mathrm{b}} : \boldsymbol{\kappa}\, \mathrm{d}\Omega + \int_{\Omega} \delta\boldsymbol{\gamma} : \mathbf{D}^{\mathrm{s}} : \boldsymbol{\gamma}\, \mathrm{d}\Omega - \int_{\Omega} \delta w p\, \mathrm{d}\Omega, \tag{6}$$

Published in : Computer methods in applied mechanics and engineering (2008), vol. 197, pp. 1184-1203
DOI: doi:10.1016/j.cma.2007.10.008
Status : Postprint (Author's version)

where the delta denotes the variation. Let us assume that the bounded domain $\boldsymbol{\Omega}$ is discretized into n_e finite elements, $\Omega \approx \Omega^h = \cup_{e=1}^{n_e} \Omega^e$. The finite element solution $\mathbf{u}^h = [w\ \beta_x\ \beta_y]^T$ of a displacement model for the Mindlin-Reissner plate is then expressed as

$$\mathbf{u}^h = \sum_{i=1}^{np} \begin{bmatrix} N_i & 0 & 0 \\ 0 & 0 & N_i \\ 0 & N_i & 0 \end{bmatrix} \mathbf{q}_i, \tag{7}$$

where np is the total number of element nodes, N_i are the bilinear shape functions associated to node i and $[w_i \theta_{xi} \theta_{yi}]^T$ are the nodal degrees of freedom of the variables $\mathbf{u}^h = [w\ \beta_x\ \beta_y]^T$ associated to node i. Then, the discrete curvature field is

$$\mathbf{k}^h = \mathbf{B}^b \mathbf{q}, \tag{8}$$

where the matrix $\mathbf{B}^b$, defined below, contains the derivatives of the shape functions. The approximation of the shear strain is written as

$$\gamma^h = \mathbf{B}^s \mathbf{q} \tag{9}$$

with

$$\mathbf{B}_i^s = \begin{bmatrix} N_{i,x} & 0 & N_i \\ N_{i,y} & -N_i & 0 \end{bmatrix}. \tag{10}$$

By substituting Eqs. (7)-(9) into Eq. (5) and with the stationarity of (5), we obtain a linear system of an individual element for the vector of nodal unknowns $\mathbf{q}$,

$$\mathbf{K}\mathbf{q} = \mathbf{g} \tag{11}$$

with the element stiffness matrix

$$\mathbf{K} = \int_{\Omega^e} (\mathbf{B}^b)^T \mathbf{D}^b \mathbf{B}^b \, d\Omega + \int_{\Omega^e} (\mathbf{B}^s)^T \mathbf{D}^s \mathbf{B}^s \, d\Omega \tag{12}$$

and the load vector

$$\mathbf{g}_i = \int_{\Omega^e} N_i \begin{bmatrix} p \\ 0 \\ 0 \end{bmatrix} d\Omega, \tag{13}$$

where

$$\mathbf{D}^b = \frac{Et^3}{12(1-\nu^2)} \begin{bmatrix} 1 & \nu & 0 \\ \nu & 1 & 0 \\ 0 & 0 & \frac{1-\nu}{2} \end{bmatrix} \quad \mathbf{D}^s = \frac{Etk}{2(1+\nu)} \begin{bmatrix} 1 & 0 \\ 0 & 1 \end{bmatrix}. \tag{14}$$

Published in : Computer methods in applied mechanics and engineering (2008), vol. 197, pp. 1184-1203
DOI: doi:10.1016/j.cma.2007.10.008
Status : Postprint (Author's version)

The element stiffness matrix **K** is symmetric and positive semi-definite. As already mentioned in the introduction, for a low-order[1] element, shear locking is observed that can be eliminated by different techniques, [3,6,28,66]. The aim of this paper is to propose a stabilized integration for a quadrilateral plate element. Therefore we will

1. Apply the curvature smoothing method which was proposed by Chen et al. [17] in meshfree methods based on the nodal integration and recently in the SFEM by Liu et al. [40] to the bending strains and

2. Adopt an independent interpolation approximation for the shear strains as in the MITC4 element [4].

In meshfree methods based on nodal integration for Mindlin-Reissner plates, convergence requires fulfilling bending exactness (BE) and thus requires the following bending integration constraint (IC) to be satisfied [56].

$$\int_{\Omega} \mathbf{B}_i^{\mathrm{b}}(\mathbf{x})\,\mathrm{d}\Omega = \int_{\Gamma} \mathbf{E}_i(\mathbf{x})\mathrm{d}\Gamma, \tag{15}$$

where $\mathbf{B}_i$ is the standard gradient matrix

$$\mathbf{B}_i^{\mathrm{b}} = \begin{bmatrix} 0 & 0 & N_{i,x} \\ 0 & -N_{i,y} & 0 \\ 0 & -N_{i,x} & N_{i,y} \end{bmatrix}, \quad \mathbf{E}_i = \begin{bmatrix} 0 & 0 & N_i n_x \\ 0 & -N_i n_y & 0 \\ 0 & -N_i n_x & N_i n_y \end{bmatrix}. \tag{16}$$

The IC criterion comes from the equilibrium of the internal and external forces of the Galerkin approximation assuming pure bending [56]. This is similar to the consistency with the pure bending deformation in the constant moment patch test in FEM.

The basic idea is to couple the MITC element with the curvature smoothing method (CSM). Therefore, smoothing cells are constructed that do not necessarily have to be coincident with the finite elements. We use a mixed variational principle based on an assumed strain field [52] and the integration is carried out either on the elements themselves, or over the smoothing cells that form a partition of the elements. The CSM is employed on each smoothing cell to normalize the local curvature and to calculate the bending stiffness matrix. The shear strains are obtained with independent interpolation functions as in the MITC element.

There are several choices for the smoothing function. For constant smoothing functions, after transforming the volume integral into a surface integral using Gauss' theorem, the surface integration over each smoothing cell becomes a line integration along its boundaries, and consequently, it is unnecessary to compute the gradient of the shape functions to obtain the curvatures and the element bending stiffness matrix. In this paper, we use 1D Gauss integration

[1] In our case a four-node quadrilateral full-integrated bilinear finite element.

Published in : Computer methods in applied mechanics and engineering (2008), vol. 197, pp. 1184-1203
DOI: doi:10.1016/j.cma.2007.10.008
Status : Postprint (Author's version)

scheme on all cell edges. The flexibility of the proposed method allows constructing four-node elements even when the elements are extremely distorted [40].

3. A formulation for four-node plate element

3.1. THE CURVATURE SMOOTHING METHOD (CSM)

The CSM was proposed by Chen et al. [17] and Wang et al. [56] as normalization of the local curvature in mesh- free methods. A curvature smoothing stabilization is created to compute the nodal curvature by a divergence estimation via a spatial averaging of the curvature fields. In other words, the domain integrals are transformed into boundary integrals. This curvature smoothing avoids the evaluation of the derivatives of the meshfree shape functions at the nodes[2], where they vanish, and thus eliminates defective modes. A curvature smoothing at an arbitrary point is given by

$$\tilde{\boldsymbol{\kappa}}^h(\mathbf{x}_C) = \int_{\Omega^h} \boldsymbol{\kappa}^h(\mathbf{x}) \Phi(\mathbf{x} - \mathbf{x}_C) \mathrm{d}\Omega, \tag{17}$$

where Φ is a smoothing function that has to satisfy the following properties [64]

$$\Phi \geqslant 0 \quad \text{and} \quad \int_{\Omega^h} \Phi \mathrm{d}\Omega = 1. \tag{18}$$

For simplicity, Φ is assumed to be a step function defined by

$$\Phi(\mathbf{x} - \mathbf{x}_C) = \begin{cases} 1/A_C, & \mathbf{x} \in \Omega_C \\ 0, & \mathbf{x} \notin \Omega_C \end{cases}, \tag{19}$$

where A_C is the area of the smoothing cell, $\Omega_C \subset \Omega^e \subset \Omega^h$ as shown in Fig. 2.

Substituting Eq. (19) into Eq. (17), and applying the divergence theorem, we obtain

$$\begin{aligned} \tilde{\kappa}_{ij}^h(\mathbf{x}_C) &= \frac{1}{2A_C} \int_{\Omega_C} \left(\frac{\partial \theta_i^h}{\partial x_j} + \frac{\partial \theta_j^h}{\partial x_i} \right) \mathrm{d}\Omega \\ &= \frac{1}{2A_C} \int_{\Gamma_C} (\theta_i^h n_j + \theta_j^h n_i) \mathrm{d}\Gamma. \end{aligned} \tag{20}$$

Next, we consider an arbitrary smoothing cell, Ω_C illustrated in Fig. 2 with boundary $\Gamma_C = \cup_{b=1}^{nb} \Gamma_C^b$, where Γ_C^b is the boundary segment of Ω_C, and *nb* is the total number of edges of each smoothing cell. The relationship between the smoothed curvature field and the nodal displacement is written by

[2] This applies only to meshfree methods that are based on a noda integration.

Published in : Computer methods in applied mechanics and engineering (2008), vol. 197, pp. 1184-1203
DOI: doi:10.1016/j.cma.2007.10.008
Status : Postprint (Author's version)

$$\tilde{\boldsymbol{\kappa}}^h = \widetilde{\mathbf{B}}_{\mathrm{C}}^{\mathrm{b}}\mathbf{q}. \quad (21)$$

The smoothed element bending stiffness matrix is obtained by

$$\begin{aligned}\tilde{\mathbf{K}}^{\mathrm{b}} &= \int_{\Omega^e} (\widetilde{\mathbf{B}}_{\mathrm{C}}^{\mathrm{b}})^{\mathrm{T}}\mathbf{D}^{\mathrm{b}}\widetilde{\mathbf{B}}_{\mathrm{C}}^{\mathrm{b}}\mathrm{d}\Omega \\ &= \sum_{C=1}^{nc} (\widetilde{\mathbf{B}}_{\mathrm{C}}^{\mathrm{b}})^{\mathrm{T}}(\mathbf{x}_{\mathrm{C}})\mathbf{D}^{\mathrm{b}}\widetilde{\mathbf{B}}_{\mathrm{C}}^{\mathrm{b}}(\mathbf{x}_{\mathrm{C}})A_{\mathrm{C}},\end{aligned} \quad (22)$$

where *nc* is the number of smoothing cells of the element, see Fig. 3.

Here, the integrands are constant over each Ω_c and the non-local curvature displacement matrix reads

$$\widetilde{B}_{Ci}^{\mathrm{b}}(\mathbf{x}_{\mathrm{C}}) = \frac{1}{A_{\mathrm{C}}}\int_{\Gamma_{\mathrm{C}}} \begin{pmatrix} 0 & 0 & N_i n_x \\ 0 & -N_i n_y & 0 \\ 0 & -N_i n_x & N_i n_y \end{pmatrix} \mathrm{d}\Gamma. \quad (23)$$

We use Gauss quadrature to evaluate (23) with one integration point over each line segment Γ_C^b :

$$\widetilde{B}_{Ci}^{\mathrm{b}}(\mathbf{x}_{\mathrm{C}}) = \frac{1}{A_{\mathrm{C}}}\sum_{b=1}^{nb} \begin{pmatrix} 0 & 0 & N_i(\mathbf{x}_{\mathrm{b}}^{\mathrm{G}})n_x \\ 0 & -N_i(\mathbf{x}_{\mathrm{b}}^{\mathrm{G}})n_y & 0 \\ 0 & -N_i(\mathbf{x}_{\mathrm{b}}^{\mathrm{G}})n_x & N_i(\mathbf{x}_{\mathrm{b}}^{\mathrm{G}})n_y \end{pmatrix} l_{\mathrm{b}}^{\mathrm{C}}, \quad (24)$$

where $\mathrm{x}_{\mathrm{b}}^{\mathrm{G}}$ and $\mathrm{l}_{\mathrm{b}}^{\mathrm{C}}$ are the midpoint (Gauss point) and the length of$\Gamma_{\mathrm{b}}^{\mathrm{C}}$, respectively.

The smoothed curvatures lead to high flexibility such as arbitrary polygonal elements, and a slight reduction in computational cost. The element is subdivided into nc non-overlapping sub-domains also called smoothing cells. Fig. 3 illustrates different smoothing cells for *nc* = 1, 2, 3 and 4 corresponding to 1-subcell, 2-subcell, 3-subcell and 4-subcell methods. The curvature is smoothed over each subcell. The values of the shape functions are indicated at the corner nodes in Fig. 3 in the format (N_1, N_2, N_3, N_4). The values of the shape functions at the integration nodes are determined based on the linear interpolation of shape functions along boundaries of the element or the smoothing cells.

Therefore the element stiffness matrix in (12) can be modified as follows:

$$\begin{aligned}\widetilde{\mathbf{K}} &= \widetilde{\mathbf{K}}^{\mathrm{b}} + \mathbf{K}^{\mathrm{s}} \\ &= \sum_{C=1}^{nc} (\widetilde{\mathbf{B}}_{\mathrm{C}}^{\mathrm{b}})^{\mathrm{T}}\mathbf{D}^{\mathrm{b}}\widetilde{\mathbf{B}}_{\mathrm{C}}^{\mathrm{b}}A_{\mathrm{C}} + \int_{\Omega^e} (\mathbf{B}^{\mathrm{s}})^{\mathrm{T}}\mathbf{D}^{\mathrm{s}}\mathbf{B}^{\mathrm{s}}\,\mathrm{d}\Omega.\end{aligned} \quad (25)$$

It can be seen that a reduced integration on the shear term $\mathbf{K}^{\mathrm{s}}$ is necessary to avoid shear locking. We will denote these elements by SC1Q4, SC2Q4, SC3Q4 and SC4Q4 corresponding to subdivision into *nc* =1,2,3 and 4 smoothing cells, Fig. 3. However, we will show that these elements fail the patch test and they exhibit an instability due to rank deficiency. Therefore, we employ a mixed

Published in : Computer methods in applied mechanics and engineering (2008), vol. 197, pp. 1184-1203
DOI: doi:10.1016/j.cma.2007.10.008
Status : Postprint (Author's version)

interpolation as in the MITC4 element and use independent interpolation fields in the natural coordinate system [4] for the approximation of the shear strains:

$$\begin{bmatrix} \gamma_x \\ \gamma_y \end{bmatrix} = \mathbf{J}^{-1} \begin{bmatrix} \gamma_\xi \\ \gamma_\eta \end{bmatrix}, \tag{26}$$

where

$$\gamma_\xi = \frac{1}{2}[(1-\eta)\gamma_\xi^{\mathrm{B}} + (1+\eta)\gamma_\xi^{\mathrm{D}}],$$
$$\gamma_\eta = \frac{1}{2}[(1-\xi)\gamma_\eta^{\mathrm{A}} + (1+\xi)\gamma_\eta^{\mathrm{C}}], \tag{27}$$

where **J** is the Jacobian matrix and the midside nodes A, B, C, D are shown in Fig. 1. Presenting $\gamma_\xi^{\mathrm{B}}, \gamma_\xi^{\mathrm{D}}$ and $\gamma_\eta^{\mathrm{A}}, \gamma_\eta^{\mathrm{C}}$ based on the discretized fields u^h, we obtain the shear matrix:

$$\mathbf{B}_i^{\mathrm{s}} = \mathbf{J}^{-1} \begin{bmatrix} N_{i,\xi} & -b_i^{12} N_{i,\xi} & b_i^{11} N_{i,\xi} \\ N_{i,\eta} & -b_i^{22} N_{i,\eta} & b_i^{21} N_{i,\eta} \end{bmatrix}, \tag{28}$$

where

$$b_i^{11} = \xi_i x_{,\xi}^M, \quad b_i^{12} = \xi_i y_{,\xi}^M, \quad b_i^{21} = \eta_i x_{,\eta}^L, \quad b_i^{22} = \eta_i y_{,\eta}^L \tag{29}$$

with $\xi_i \in \{-1, 1, 1, -1\}$, $\eta_i \in \{-1, -1, 1, 1\}$ and $(i, M, L) \in \{(1, B, A); (2, B, B); (3, D, C); (4, D, A)\}$. Note that the shear term $\mathbf{K}^{\mathrm{s}}$ is still computed by 2 x 2 Gauss quadrature while the element bending stiffness $\mathbf{K}^{\mathrm{b}}$ in Eq. (12) is replaced by the smoothed curvature technique on each smoothing cell of the element.

3.2. HU-WASHIZU VARIATIONAL FORMULATION

We use a modified Hu-Washizu variational formulation [58] given for an individual element by

$$\begin{aligned} \Pi_{\mathrm{HW}}^e(w, \tilde{\boldsymbol{\kappa}}, \mathbf{M}) = & \frac{1}{2}\int_{\Omega^e} \tilde{\boldsymbol{\kappa}} : \mathbf{D}^{\mathrm{b}} : \tilde{\boldsymbol{\kappa}} \, \mathrm{d}\Omega \\ & - \int_{\Omega^e} \mathbf{M} : (\tilde{\boldsymbol{\kappa}} - \boldsymbol{\kappa}) \, \mathrm{d}\Omega + \frac{1}{2}\int_{\Omega^e} \boldsymbol{\gamma} : \mathbf{D}^{\mathrm{s}} : \boldsymbol{\gamma} \, \mathrm{d}\Omega \\ & - \int_{\Omega^e} wp \, \mathrm{d}\Omega, \end{aligned} \tag{30}$$

where **M** is the moment tensor. Partitioning the element into *nc* sub-cells such that the sub-cells are not overlapping and form a partition of the element Ω^{e}, $\Omega^{\mathrm{e}} = \cup_{\mathrm{ic}=1}^{\mathrm{nc}} \Omega_{\mathrm{ic}}^{\mathrm{e}}$, the functional energy, $\Pi_{\mathrm{HW}}^{\mathrm{e}}$, can be rewritten as

Published in : Computer methods in applied mechanics and engineering (2008), vol. 197, pp. 1184-1203
DOI: doi:10.1016/j.cma.2007.10.008
Status : Postprint (Author's version)

$$\begin{aligned}\Pi^{e}_{\mathrm{HW}}(w,\tilde{\boldsymbol{\kappa}},\mathbf{M}) = &\frac{1}{2}\sum_{ic=1}^{nc}\int_{\Omega^{e}_{ic}}\tilde{\boldsymbol{\kappa}}_{ic}:\mathbf{D}^{\mathrm{b}}:\tilde{\boldsymbol{\kappa}}_{ic}\,\mathrm{d}\Omega^{e}_{ic}\\ &-\sum_{ic=1}^{nc}\int_{\Omega^{e}_{ic}}\mathbf{M}:(\tilde{\boldsymbol{\kappa}}-\boldsymbol{\kappa})\mathrm{d}\Omega^{e}_{ic}\\ &+\frac{1}{2}\int_{\Omega^{e}}\boldsymbol{\gamma}:\mathbf{D}^{\mathrm{s}}:\boldsymbol{\gamma}\,\mathrm{d}\Omega-\int_{\Omega^{e}}wp\,\mathrm{d}\Omega,\end{aligned} \tag{31}$$

where

$$\tilde{\boldsymbol{\kappa}}_{ic}=\frac{1}{A_{ic}}\int_{\Omega^{e}_{ic}}\boldsymbol{\kappa}(\mathbf{x})\mathrm{d}\Omega^{e}_{ic}\quad\text{and}\quad A^{e}=\sum_{ic=1}^{nc}A_{ic} \tag{32}$$

with A_{ic} is the area of the smoothing cell, Ω^{e}_{ic}.

To reduce Π^{e}_{HW} from a three-field potential to a two- field potential, we need to find a strict condition on the smoothing cells Ω_C for the orthogonality condition [52,53]:

$$\int_{\Omega^{e}}\mathbf{M}:\hat{\boldsymbol{\kappa}}\,\mathrm{d}\Omega=\int_{\Omega^{e}}\mathbf{M}:(\tilde{\boldsymbol{\kappa}}-\boldsymbol{\kappa})\,\mathrm{d}\Omega=0 \tag{33}$$

is satisfied. By substituting **M** through the constitutive relation $M=D^{b}{}_{\tilde{k}}$, we rewrite the orthogonality condition:

$$\begin{aligned}\int_{\Omega^{e}}\mathbf{M}:\hat{\boldsymbol{\kappa}}\,\mathrm{d}\Omega&=\sum_{ic=1}^{nc}\int_{\Omega^{e}_{ic}}\mathbf{D}^{\mathrm{b}}\tilde{\boldsymbol{\kappa}}:(\tilde{\boldsymbol{\kappa}}-\boldsymbol{\kappa})\mathrm{d}\Omega^{e}_{ic}\\ &=\sum_{ic=1}^{nc}\int_{\Omega^{e}_{ic}}\mathbf{D}^{\mathrm{b}}\tilde{\boldsymbol{\kappa}}:\left(\frac{1}{A_{\mathrm{C}}}\int_{\Omega_{\mathrm{C}}}\boldsymbol{\kappa}\,\mathrm{d}\Omega_{\mathrm{C}}-\boldsymbol{\kappa}\right)\mathrm{d}\Omega^{e}_{ic}\\ &=\sum_{ic=1}^{nc}\mathbf{D}^{\mathrm{b}}\tilde{\boldsymbol{\kappa}}:\int_{\Omega^{e}_{ic}}\left(\frac{1}{A_{\mathrm{C}}}\int_{\Omega_{\mathrm{C}}}\boldsymbol{\kappa}\,\mathrm{d}\Omega_{\mathrm{C}}-\boldsymbol{\kappa}\right)\mathrm{d}\Omega^{e}_{ic}\\ &=\sum_{ic=1}^{nc}\mathbf{D}^{\mathrm{b}}\tilde{\boldsymbol{\kappa}}:\left(\frac{\int_{\Omega^{e}_{ic}}\mathrm{d}\Omega^{e}_{ic}}{A_{\mathrm{C}}}\int_{\Omega_{\mathrm{C}}}\boldsymbol{\kappa}\,\mathrm{d}\Omega_{\mathrm{C}}-\int_{\Omega^{e}_{ic}}\boldsymbol{\kappa}\mathrm{d}\Omega^{e}_{ic}\right)\\ &=\sum_{ic=1}^{nc}\mathbf{D}^{\mathrm{b}}\tilde{\boldsymbol{\kappa}}:\left(\frac{A_{ic}}{A_{\mathrm{C}}}\int_{\Omega_{\mathrm{C}}}\boldsymbol{\kappa}\mathrm{d}\Omega_{\mathrm{C}}-\int_{\Omega^{e}_{ic}}\boldsymbol{\kappa}\,\mathrm{d}\Omega^{e}_{ic}\right),\end{aligned} \tag{34}$$

where $\Omega_C \subset \Omega^e$ is a smoothed curvature field defined for every $\tilde{\mathrm{k}}=\frac{1}{A_C}\int_{\Omega_C}\mathrm{k}(\mathrm{x})\mathrm{d}\Omega$ and the smoothed $\tilde{\mathrm{k}}$ curvature does not depend on the integration after processing a smoothed operator, i.e.,

$$\int_{\Omega^{e}_{ic}}\mathbf{D}^{\mathrm{b}}\tilde{\boldsymbol{\kappa}}\,\mathrm{d}\Omega^{e}_{ie}=\mathbf{D}^{\mathrm{b}}\tilde{\boldsymbol{\kappa}}A_{ic}$$

with

$$A_{\mathrm{C}}=A_{ic}\quad\text{and}\quad\Omega_{\mathrm{C}}\equiv\Omega^{e}_{ic}. \tag{35}$$

Published in : Computer methods in applied mechanics and engineering (2008), vol. 197, pp. 1184-1203
DOI: doi:10.1016/j.cma.2007.10.008
Status : Postprint (Author's version)

If Ω_c coincides with Ω_{ic}^e, the orthogonality condition (33) is met and the three-field potential is reduced to a two-field potential:

$$\Pi_{\mathrm{HW}}^e(w,\tilde{\boldsymbol{\kappa}}) = \frac{1}{2}\sum_{ic=1}^{nc}\int_{\Omega_{ic}^e}\tilde{\boldsymbol{\kappa}}_{ic} : \mathbf{D}^{\mathrm{b}} : \tilde{\boldsymbol{\kappa}}_{ic}\,\mathrm{d}\Omega_{ic}^e + \frac{1}{2}\int_{\Omega^e}\boldsymbol{\gamma} : \mathbf{D}^{\mathrm{s}} : \boldsymbol{\gamma}\,\mathrm{d}\Omega - \int_{\Omega^e} wp\,\mathrm{d}\Omega. \tag{36}$$

Now we show that the proposed total energy approaches the total potential energy variational principle (TPE) when *nc* tends to infinity. Based on the definition of the double integral formula, when $nc \to \infty, A_{ic} \to dA_{ic}$ - an infinitesimal area containing point $\mathbf{x}_{ic}$, applying the mean value theorem for the smoothed strain,

$$\tilde{\boldsymbol{\kappa}}_{ic} = \int_{\Omega_{ic}^e}\frac{\boldsymbol{\kappa}(\mathbf{x})}{A_{ic}}\,\mathrm{d}\Omega_{ic}^e \to \boldsymbol{\kappa}(\mathbf{x}_{ic}), \tag{37}$$

where **k(x)** is assumed to be a continuous function. Eq. (37) states that the average value of **k(x)** over a domain Ω_{ic}^e approaches its value at the converged point $\mathbf{x}_{ic}$.

Taking the limit of Π_{HW}^e when the number of subcells tends to infinity,

$$\begin{aligned}
&\lim_{nc\to\infty}\Pi_{\mathrm{HW}}^e(w,\tilde{\boldsymbol{\kappa}})\\
&= \frac{1}{2}\lim_{nc\to\infty}\sum_{ic=1}^{nc}\int_{\Omega_{ic}^e}\mathbf{D}^{\mathrm{b}} : \left(\int_{\Omega_{ic}^e}\frac{\boldsymbol{\kappa}(\mathbf{x})}{A_{ic}}\,\mathrm{d}\Omega_{ic}^e\right) : \left(\int_{\Omega_{ic}^e}\frac{\boldsymbol{\kappa}(\mathbf{x})}{A_{ic}}\,\mathrm{d}\Omega_{ic}^e\right)\mathrm{d}\Omega_{ic}^e\\
&\quad + \frac{1}{2}\int_{\Omega^e}\boldsymbol{\gamma} : \mathbf{D}^{\mathrm{s}} : \boldsymbol{\gamma}\,\mathrm{d}\Omega - \int_{\Omega^e} wp\,\mathrm{d}\Omega\\
&= \frac{1}{2}\lim_{nc\to\infty}\sum_{ic=1}^{nc}\mathbf{D}^{\mathrm{b}} : \boldsymbol{\kappa}(\mathbf{x}_{ic}) : \boldsymbol{\kappa}(\mathbf{x}_{ic})\mathrm{d}A_{ic}\\
&\quad + \frac{1}{2}\int_{\Omega^e}\boldsymbol{\gamma} : \mathbf{D}^{\mathrm{s}} : \boldsymbol{\gamma}\,\mathrm{d}\Omega - \int_{\Omega^e} wp\,\mathrm{d}\Omega\\
&= \frac{1}{2}\int_{\Omega^e}\mathbf{D}^{\mathrm{b}} : \boldsymbol{\kappa}(\mathbf{x}) : \boldsymbol{\kappa}(\mathbf{x})\mathrm{d}\Omega\\
&\quad + \frac{1}{2}\int_{\Omega^e}\boldsymbol{\gamma} : \mathbf{D}^{\mathrm{s}} : \boldsymbol{\gamma}\,\mathrm{d}\Omega - \int_{\Omega^e} wp\,\mathrm{d}\Omega\\
&= \Pi_{\mathrm{TPE}}^e(w,\boldsymbol{\beta}).
\end{aligned} \tag{38}$$

The above proves that the total potential energy variational principle is recovered from the proposed variational formulation as *nc* tends to infinity.

Published in : Computer methods in applied mechanics and engineering (2008), vol. 197, pp. 1184-1203
DOI: doi:10.1016/j.cma.2007.10.008
Status : Postprint (Author's version)

4. Numerical results

We will test our new element for different numbers of smoothing cells and call our element MISCk (mixed interpolation and smoothed curvatures) with $k \in \{1,2,3,4\}$ smoothing cells for the bending terms. For instance, the MISC1 element is the element with only one smoothing cell to integrate the bending part of the element stiffness matrix. We will compare our results to the results obtained with the reduced/selective integrated quadrilateral element (Q4-R), the MITC4 element and with several other elements in the literatures.

4.1. PATCH TEST

The patch test was introduced by Bruce Irons and Bazeley [7] to check the convergence of finite elements. It is checked if the element is able to reproduce a constant distribution of all quantities for arbitrary meshes. It is important that one element is completely surrounded by neighboring elements in order to test if a rigid body motion is modelled correctly, Fig. 4. The boundary deflection is assumed to be $w = \frac{1}{2}(1 + x + 2y + x^2 + xy + y^2)$ [18]. The results are shown in Table 1. While the MITC4 element and the MISCk elements pass the patch test, the Q4-R element and the SC1Q4, SC2Q4, SC3Q4, SC4Q4 elements fail the patch test. Note that also the fully integrated Q4 element (on both the bending and the shear terms) does not pass the patch test.

4.2. A SENSITIVITY TEST OF MESH DISTORTION

Consider a clamped square plate subjected to a center point *F* or uniform load *p* shown in Fig. 5. The geometry parameters and the Poisson's ratio are: length *L*, thickness *t*, and ν= 0.3. Due to its symmetry, only a quarter (lower-left) of the plate is modelled with a mesh of 8 x 8 elements. To study the effect of mesh distortion on the results, interior nodes are moved by an irregularity factor s. The coordinates of interior nodes is perturbed as follows [40]:

$$x' = x + r_c s \Delta x,$$
$$y' = y + r_c s \Delta y, \quad (39)$$

where r_c is a generated random number given values between — 1.0 and 1.0, $s \in [0,0.5]$ is used to control the shapes of the distorted elements and Δx, Δy are initial regular element sizes in the x- and y-directions, respectively.

For the concentrated center point load *F,* the influence of the mesh distortion on the center deflection is given in Fig. 6 for a thickness ratio of (t/L = 0.01 and 0.001). The results of our presented method are more accurate than those of the Q4-R element and the MITC4 element, especially for extremely distorted meshes. Here, the MISC1 element gives the best result. However, this element contains two zero-energy modes. In simple problems, these hourglass modes can be automatically eliminated by the boundary conditions. However, this is not in general the case. Otherwise, the

Published in : Computer methods in applied mechanics and engineering (2008), vol. 197, pp. 1184-1203
DOI: doi:10.1016/j.cma.2007.10.008
Status : Postprint (Author's version)

MISC2, MISC3 and MISC4 elements retain a sufficient rank of the element stiffness matrix and give excellent results.

Let us consider a thin plate with (t/L = 0.001) under uniform load as shown Fig. 5a. The numerical results of the central deflections are shown in Table 2 and Fig. 7 and compared to other elements. For the case $s = 0$, it can be seen that the MISCk elements yield similar or slightly more accurate results than the other elements. Moreover, all proposed elements lead to slightly better results than the elements used for comparison, especially for distorted meshes, $s > 0$.

4.3. SQUARE PLATE SUBJECTED TO A UNIFORM LOAD OR A POINT LOAD

Figs. 5a and 13 are the model of a square plate with clamped and simply supported boundary conditions, respectively, subjected to a uniform load $p = 1$ or a central load $F = 16.3527$. The material parameters are given by Young's modulus $E = 1{,}092{,}000$ and Poisson's ratio $\nu = 0.3$. Uniform meshes with $N = 2, 4, 8, 16, 32$ are used and symmetry conditions are exploited.

For a clamped case, Fig. 8 illustrates the convergence of the normalized deflection and the normalized moment at the center versus the mesh density N for a relation $t/L = 0.01$. Even for very coarse meshes, the deflection tends to the exact solution. For the finest mesh, the displacement slightly (.06%) exceeds the value of the exact solution. The bending moment converges to the analytical value. The rate of convergence in the energy norm is presented in Fig. 9 and is for all elements equal to 1.1 but the MISCk elements are more accurate than the MITC4 element in energy.

Tables 3 and 4 show the performance of the plate element for different thickness ratios, $t/L = 10^{-1}$-10^{-5}. No shear locking is observed. In addition, it is observed that the MIS- Ck elements improve the solutions with coarse meshes while for fine meshes all elements lead to very similar results.

Next we consider a sequence of distorted meshes with 25, 81, 289 and 1089 nodes as shown in Fig. 10. The numerical results in terms of the error in the central displacement and the strain energy are illustrated in Fig. 11. All proposed elements give stable and accurate results. Especially for coarse meshes, the MISCk elements are more accurate than the MITC4 element; a reason for this may be that for our finest meshes, fewer elements are distorted in comparison to coarse meshes.

Now we will test the computing time for the clamped plate analyzed above. The program is compiled by a personal computer with Pentium(R)4, CPU - 3.2 GHz and RAM - 512 MB. The computational cost to set up the global stiffness matrix and to solve the algebraic equations is illustrated in Fig. 12. The MISCk elements and the MITC4 element give nearly the same CPU time for coarse meshes where the MISCk elements are more accurate. From the plots, we can conjecture that for finer meshes, the MITC4 element is computationally more expensive than the MISCk element, and the MISCk elements are generally more accurate. The lower computational cost comes from the fact that no computation of the Jacobian matrix is necessary for the MISCk elements while the MITC4 element needs to determine the Jacobian determinant, the inverse of the Jacobian matrix (transformation of two coordinates; global coordinate and local coordinate) and then the stiffness matrix is calculated by 2 x 2 Gauss points. Previously, the same tendency was observed for the standard (Q4 element), see [40] for details.

Published in : Computer methods in applied mechanics and engineering (2008), vol. 197, pp. 1184-1203
DOI: doi:10.1016/j.cma.2007.10.008
Status : Postprint (Author's version)

For a simply supported plate subjected to central concentrated load, the same tendencies as described above are observed. Exemplarily, we will show the results of the normalized deflection in Fig. 14a for the uniform meshes and in Fig. 14b for the distorted meshes illustrated in Fig. 10.

The numerical results for a simply supported plate subjected to a uniform load are presented in Tables 5 and 6 and Figs. 15 and 16 for a regular mesh. We note that the MISCk elements are more accurate than the MITC4 element but show the same convergence rate in energy. We also see that no shear locking occurs with decreasing thickness. Also, for all elements presented, the displacement results do not seem to be influenced by the value of the thickness ratio, at least in the range $t/L \in [10^{-5},10^{-3}]$. The moments remain accurate throughout the range of thickness ratios that we considered.

4.4. SKEW PLATE SUBJECTED TO A UNIFORM LOAD

4.4.1. RAZZAQUE'S SKEW PLATE MODEL

Let us consider a rhombic plate subjected to a uniform load $p = 1$ as shown in Fig. 17a. This plate was originally studied by Razzaque [51]. Dimensions and boundary conditions are specified in Fig. 17a, too. Geometry and material parameters are length $L = 100$, thickness $t = 0.1$, Young's modulus $E = 1{,}092{,}000$ and Poisson's ratio $\nu = 0.3$. The results in Table 7 show that the accuracy of the presented method is always better than that of the MITC4 element. Fig. 18 illustrates the contribution of the von Mises stresses and the level lines for Razzaque's skew plate with our MISC4 element.

4.4.2. MORLEY'S SKEW PLATE MODEL

The set-up of a skew plate is shown in Fig. 17b. This example was first studied by Morley [45]. The geometry and material parameters are length $L = 100$, thickness t, Young's modulus $E = 1{,}092{,}000$, Poisson's ratio $\nu = 0.3$ and a uniform load $p = 1$. The values of the deflection at the central point are given in Fig. 20 for different plate thicknesses. The MISCk elements show remarkably good results compared the MITC4 element. The distribution of the von Mises stresses and the level lines are illustrated in Fig. 19. It is evident that this problem has a corner singularity. An adaptive approach might be useful to optimize the computational cost.

As we prove mathematically and show numerically in a short communication to be published in Computer Methods in Applied Mechanics and Engineering, in the context of continuum elements, the smoothed finite element method yields solutions comprised between the standard, displacement based FEM and equilibrium, stress based elements. The equilibrium method is recovered when one smoothing cell is used and the displacement method is found in the limit where the number of smoothing cells tends to infinity. It appears like this property could also be verified in the context of plate analysis. At least, the results in Fig. 20 tend to indicate that the higher the number of smoothing cells, the closer the solution is to the MITC4 elements, with almost identical behaviour for 4 smoothing cells. On the contrary, it is interesting to note that the one-subcell element (MISC1) overestimates the energy (similarly to equilibrium methods).

Published in : Computer methods in applied mechanics and engineering (2008), vol. 197, pp. 1184-1203
DOI: doi:10.1016/j.cma.2007.10.008
Status : Postprint (Author's version)

4.5. CORNER SUPPORTED SQUARE PLATE

Consider a corner supported plate subjected to a uniform load p = 0.03125 with edge length L = 24 and thickness t = 0.375. This example is often studied to test the existence of spurious energy modes. The material parameters are Young's modulus E = 430,000 and Poisson's ratio ν = 0.38. The shear correction factor was set to a value of k = 1000. A symmetric model with an initial mesh of 8 x 8 elements is shown in Fig. 21. Table 8 shows the convergence of the center deflection. We note that even our rank-deficient MISC1 element gives stable and very accurate results.

We have also carried out a frequency analysis. The mass density is chosen to be ρ = 0.001 and the normalized frequencies are $\bar{\omega} = \omega L^2 (D/t\rho)^{-1/2}$. The results are illustrated in Table 9 for two mesh densities (6 x 6 and 32 x 32). It can be seen that all proposed elements give stable and accurate solutions.

4.6. CLAMPED CIRCULAR PLATE SUBJECTED TO A CONCENTRATED LOAD

Let us consider a clamped circular plate with radius R = 5 subjected to a point load F = 1 at the center. The material and geometric parameters are Young's modulus E = 10.92, Poisson's ratio ν= 0.3 and the thickness of the plate is 1. The analytical deflection for this problem is

$$w(r) = \frac{FR^2}{16\pi D}\left(1 - \frac{r^2}{R^2} + \frac{2r^2}{R^2}\ln\frac{r}{R} - \frac{8D}{kGtR^2}\ln\frac{r}{R}\right). \quad (40)$$

A discretization of this problem with 48 elements is illustrated in Fig. 22. We exploited the symmetry of the plate and modelled only one quarter. Because of the singularity at the center, the normalized central deflection is evaluated at the radius $r = 10^{-3}R$. The numerical results are summarized in Table 10 and Fig. 23. The MITC4 and MISCk elements converge to the exact value with refined meshes. However, the convergence in the central deflection is slow due to the singularity at the center. To increase the convergence rate of the problem, an adaptive local refinement procedure (or XFEM-like enrichment) should be considered in the future. If the ratio r/R is large enough, the numerical results are very close to the analytical solution.

5. Closure and opening

A quadrilateral plate element based on a mixed interpolation with smoothed curvatures has been proposed. Except for the MISC1 element that exhibits two zeroenergy modes, the MISC2, MISC3 and MISC4 elements maintain a sufficient rank and no zero-energy modes are present. Moreover, all proposed elements do not exhibit shear locking in the limit to thin plates. It is also shown that the MISCk element passes the patch test. For regular, non-distorted meshes, in comparison to the well known MITC4 element, the proposed elements are slightly more accurate, for all examples tested. But their most promising feature is their improved performance for irregular meshes or coarse meshes and their lower computational cost (about 25% in our implementation. No analytical complexity analysis is available to date) The element with the best performance is the MISC1

Published in : Computer methods in applied mechanics and engineering (2008), vol. 197, pp. 1184-1203
DOI: doi:10.1016/j.cma.2007.10.008
Status : Postprint (Author's version)

element but it exhibits two zero-energy modes. However, for the examples tested here, no instabilities were observed. The elimination of the zero-energy modes of our MISC1 elements will be investigated in the future. The MISC2 element is almost of the same accuracy as the MISC1 element and it is stable but it slightly slower.

We believe that our element is especially useful for certain types of problems where locally large deformations or strains occur, e.g. ductile cracking where crack initiation and propagation occurs under large strains and large deformation. It is important to retain accuracy in a local region before cracking happens in order to obtain the correct crack path [16,50]. This will be investigated in the future using open source XFEM libraries [15,23]. The MISCk elements can be extended to non-linear material models including strong discontinuities such as in the eXtended finite element method (XFEM) introduced by [8,9,43,44] and improved to handle complex industrial structures in [14,11] and, later, [60-63]. For discontinuous problems, an adaptive procedure might be useful as well, for instance, following the seminal work presented in [12,13,22]. We expect the h-adaptivity procedure to be simplified compared to standard finite element formulations, because remeshing will not be as severely constrained by mesh quality requirements as in standard finite element methods.

Another study will concern the shear term. By replacing 2 x 2 Gauss integration on the shear term with a reduced integration with stabilization, we expect the element to be even better suited to handle arbitrary mesh distortions

Published in : Computer methods in applied mechanics and engineering (2008), vol. 197, pp. 1184-1203
DOI: doi:10.1016/j.cma.2007.10.008
Status : Postprint (Author's version)

Figure 1. *Assumption of shear deformations for quadrilateral plate element.*

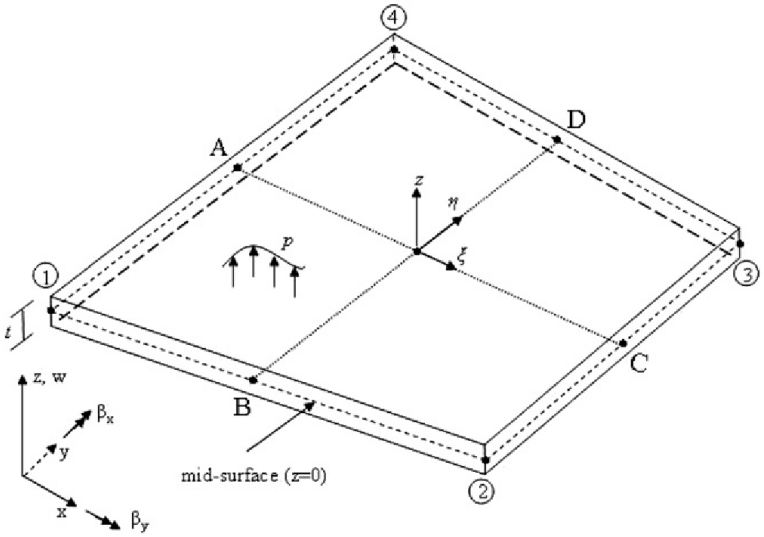

Figure 2. *Example of finite elements mashes and smoothing cells*

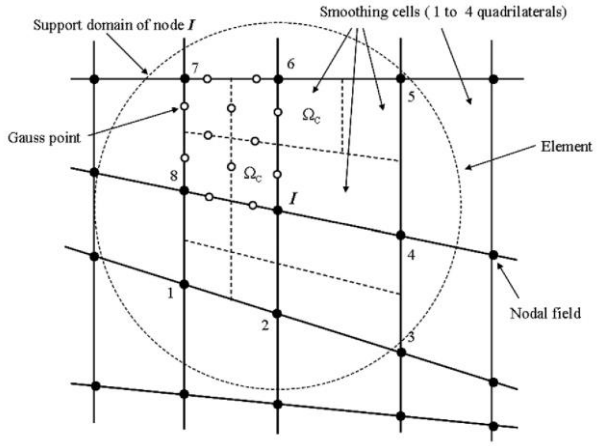

Figure 3. *Division of an element into smoothing cells (nc) and the value of the shape function along the boundaries of cells: k-subcell stands for the shape function of the MISCk element, k = 1-4.*

Published in : Computer methods in applied mechanics and engineering (2008), vol. 197, pp. 1184-1203
DOI: doi:10.1016/j.cma.2007.10.008
Status : Postprint (Author's version)

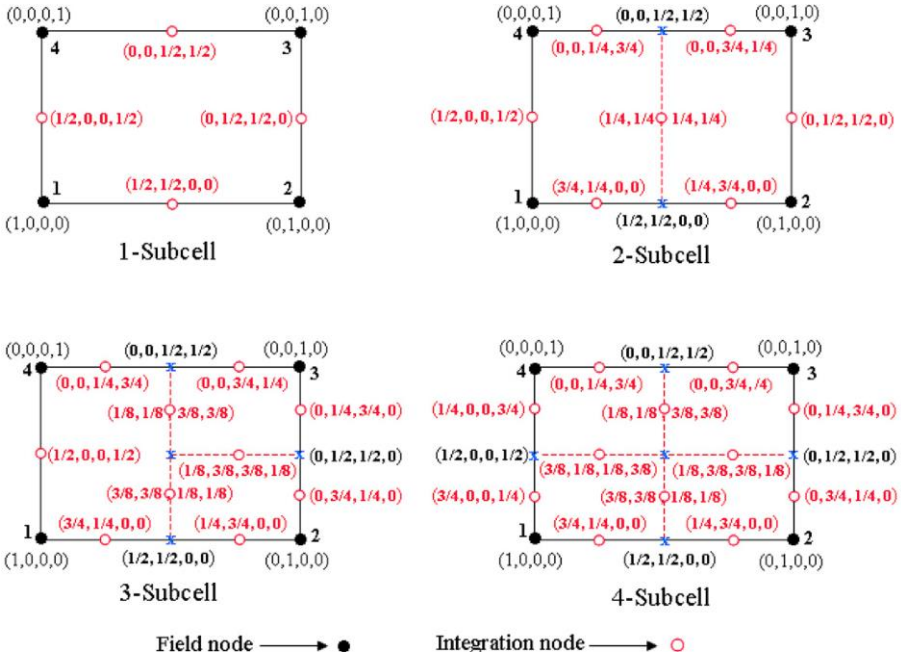

Published in : Computer methods in applied mechanics and engineering (2008), vol. 197, pp. 1184-1203
DOI: doi:10.1016/j.cma.2007.10.008
Status : Postprint (Author's version)

Figure 4. *Patch test of elements*

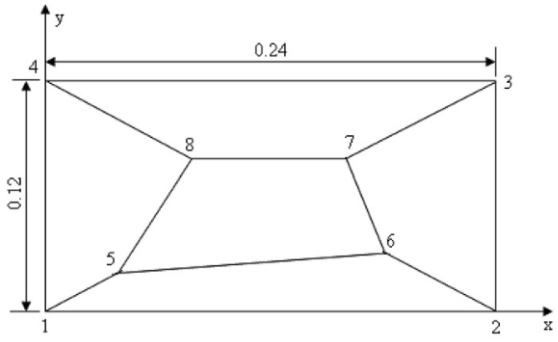

Node	coordinates	
1	0.0	0.0
2	0.24	0.0
3	0.24	0.12
4	0.0	0.12
5	0.04	0.02
6	0.18	0.03
7	0.16	0.08
8	0.08	0.08

Figure 5. *Effect of mesh distortion for a clamped square plate: (a) clamped plate model; (b) s = 0.3; (c) s = 0.4; and (d) s = 0.5.*

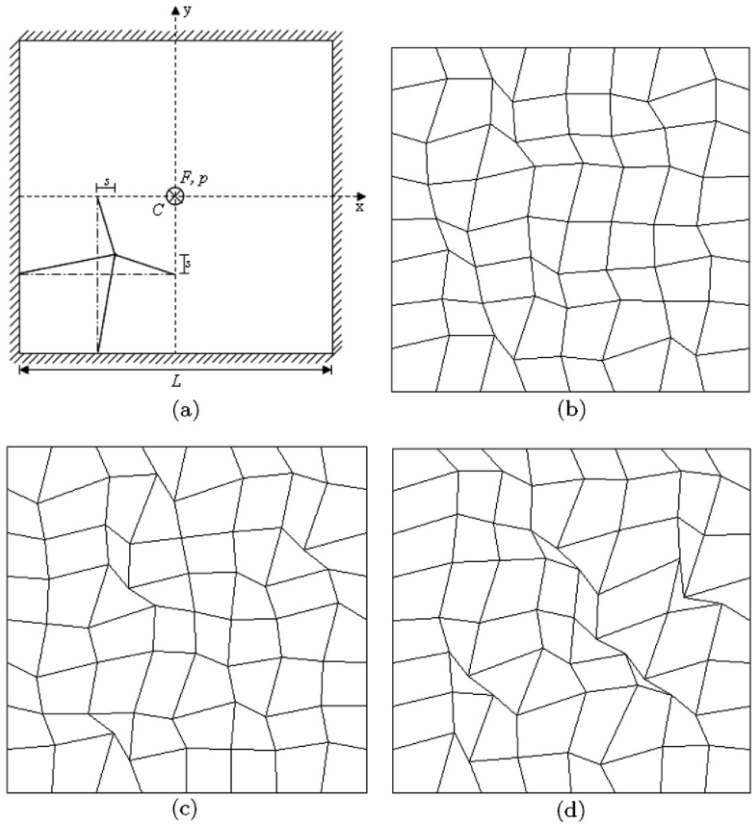

Figure 6. *The normalized center deflection with influence of mesh distortion for a clamped square plate subjected to a concentrated load: (a) t/L = 0.01 and (b) tlL = 0.001.*

Published in : Computer methods in applied mechanics and engineering (2008), vol. 197, pp. 1184-1203
DOI: doi:10.1016/j.cma.2007.10.008
Status : Postprint (Author's version)

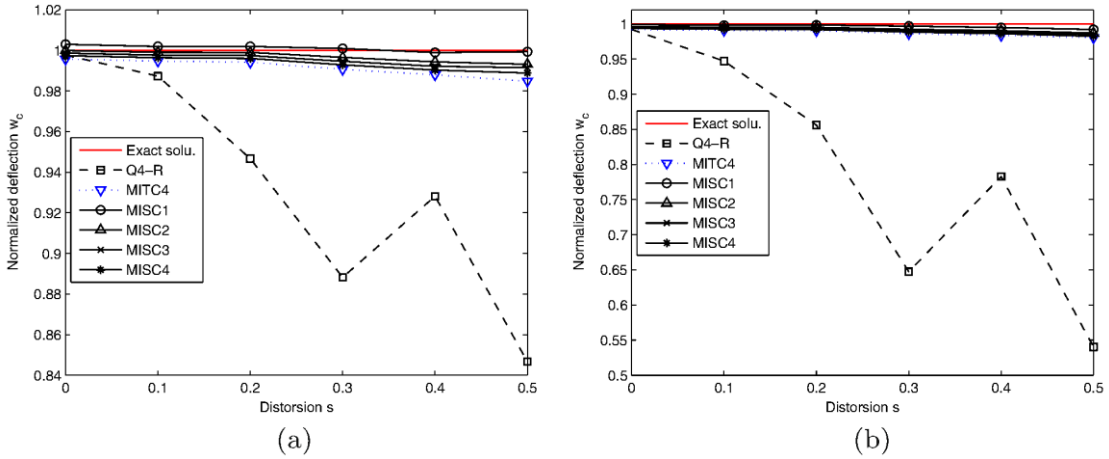

Figure 7. *Comparison of other elements through the center deflection with mesh distortion.*

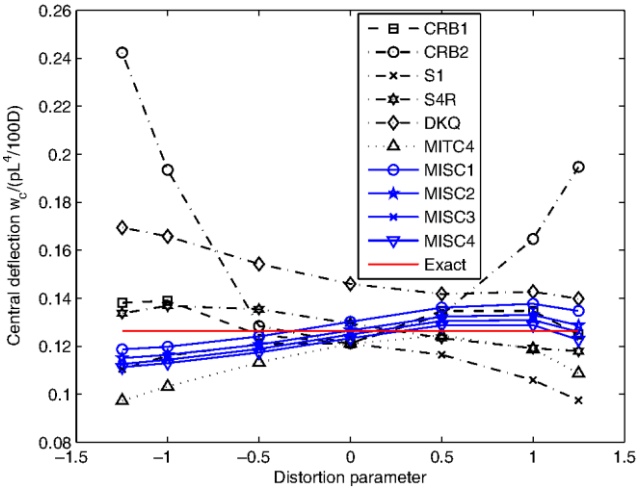

Figure 8. *Normalized deflection and moment at center of clamped square plate subjected to uniform load.*

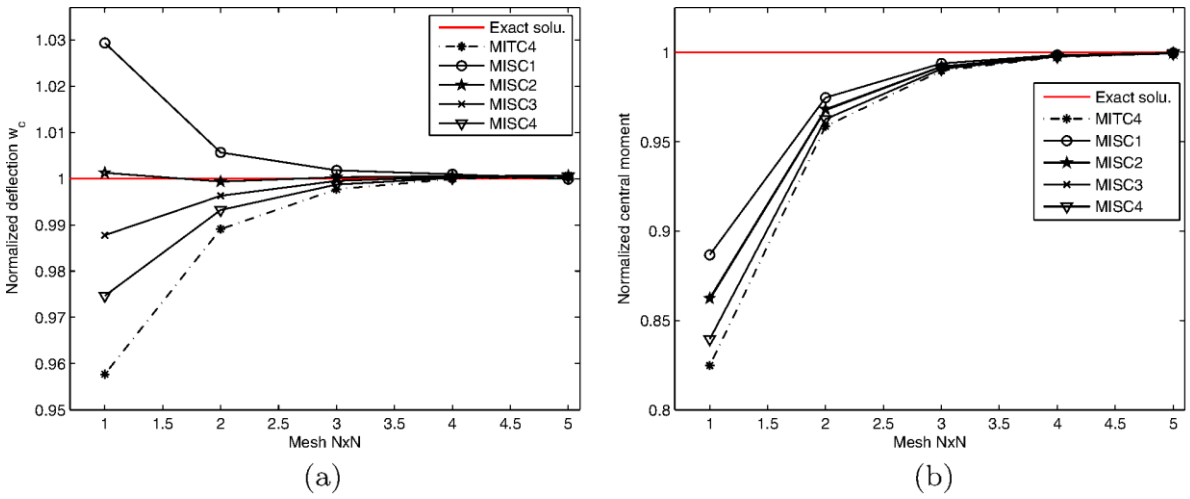

Published in : Computer methods in applied mechanics and engineering (2008), vol. 197, pp. 1184-1203
DOI: doi:10.1016/j.cma.2007.10.008
Status : Postprint (Author's version)

Figure 9. *Rate of convergence in energy norm versus with number of nodes for clamped square plate subjected to uniform load.*

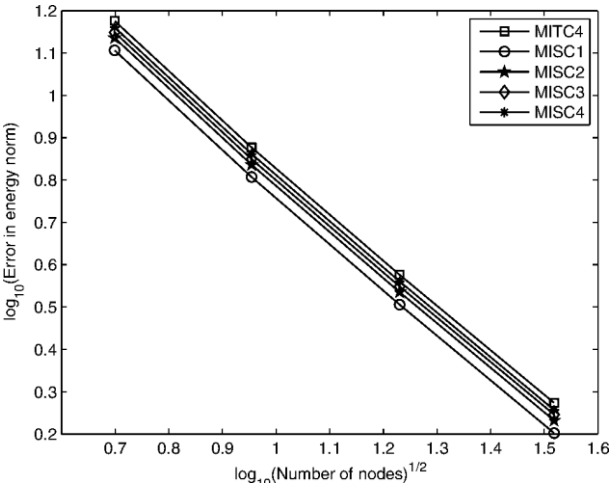

Figure 10. *Analysis of clamped plate with irregular elements: (a) 25; (b) 64; (c) 256; and (d) 1024*

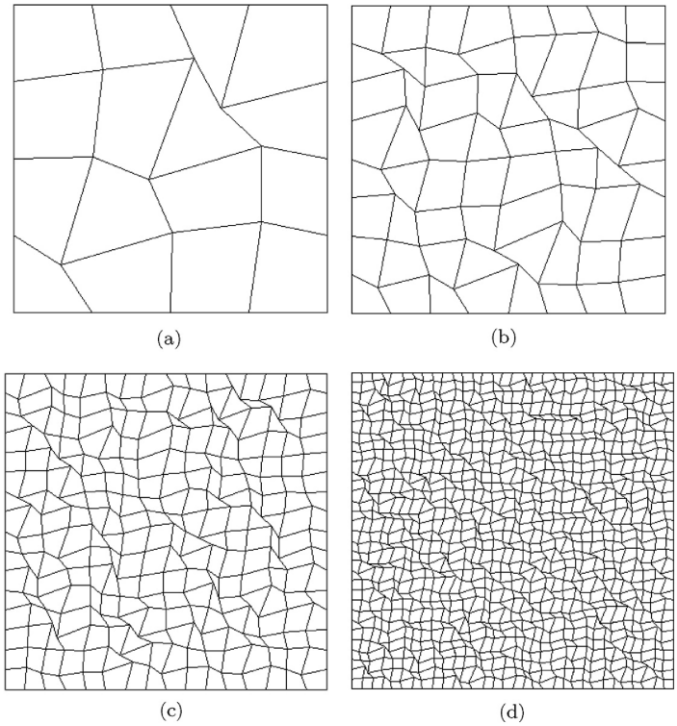

Published in : Computer methods in applied mechanics and engineering (2008), vol. 197, pp. 1184-1203
DOI: doi:10.1016/j.cma.2007.10.008
Status : Postprint (Author's version)

Figure 11. *The convergence test of thin clamped plate (t/L = 0.001) (with irregular elements: (a) the deflection; (b) the strain energy).*

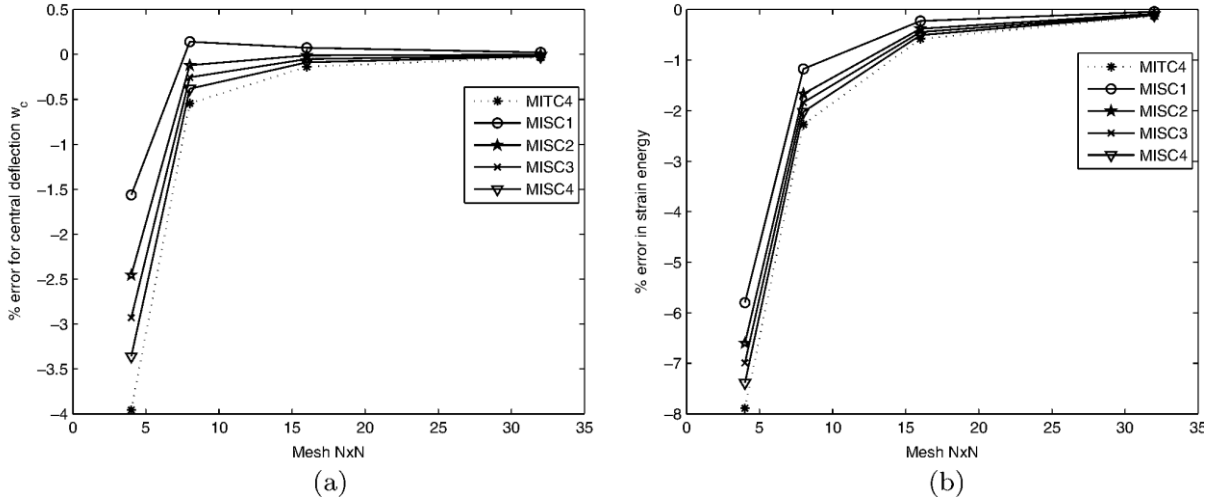

Figure 12. *Computational cost for establishing the global stiffness matrix and solving system equations of clamped plate subjected to a uniform load.*

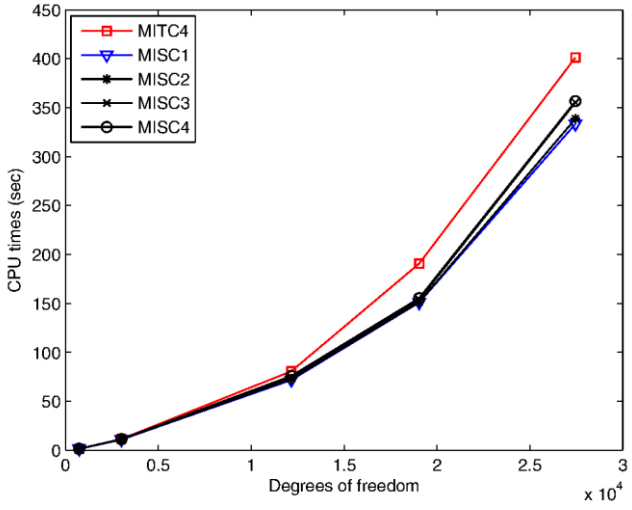

Published in : Computer methods in applied mechanics and engineering (2008), vol. 197, pp. 1184-1203
DOI: doi:10.1016/j.cma.2007.10.008
Status : Postprint (Author's version)

Figure 13. *A simply supported square plate subjected to a point load or a uniform load.*

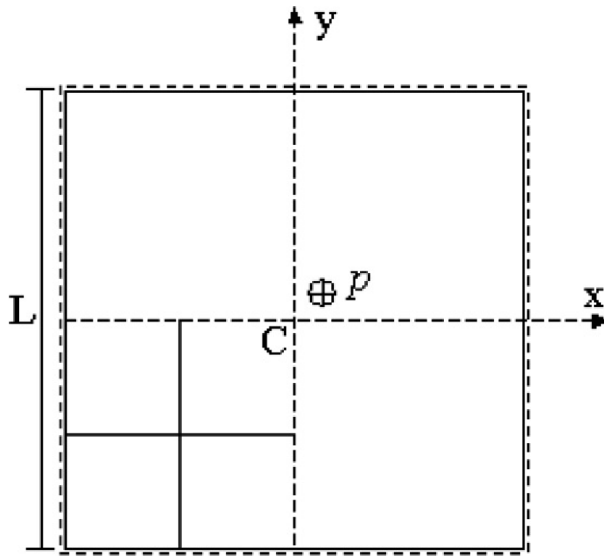

Figure 14. *Normalized deflection at the center of the simply supported square plate subjected to a center load.*

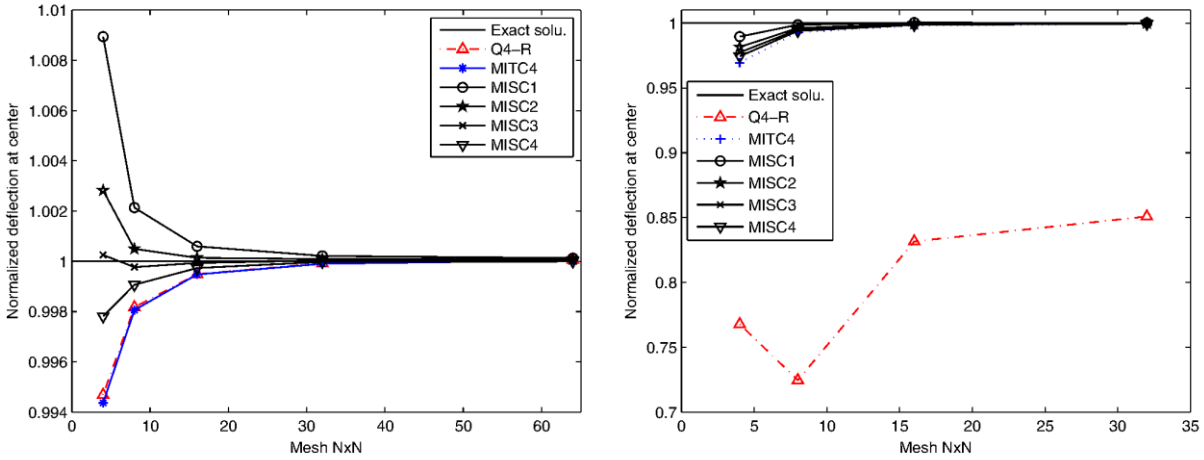

Published in : Computer methods in applied mechanics and engineering (2008), vol. 197, pp. 1184-1203
DOI: doi:10.1016/j.cma.2007.10.008
Status : Postprint (Author's version)

Figure 15. *Normalized deflection and moment at center of simply support square plate subjected to uniform load.*

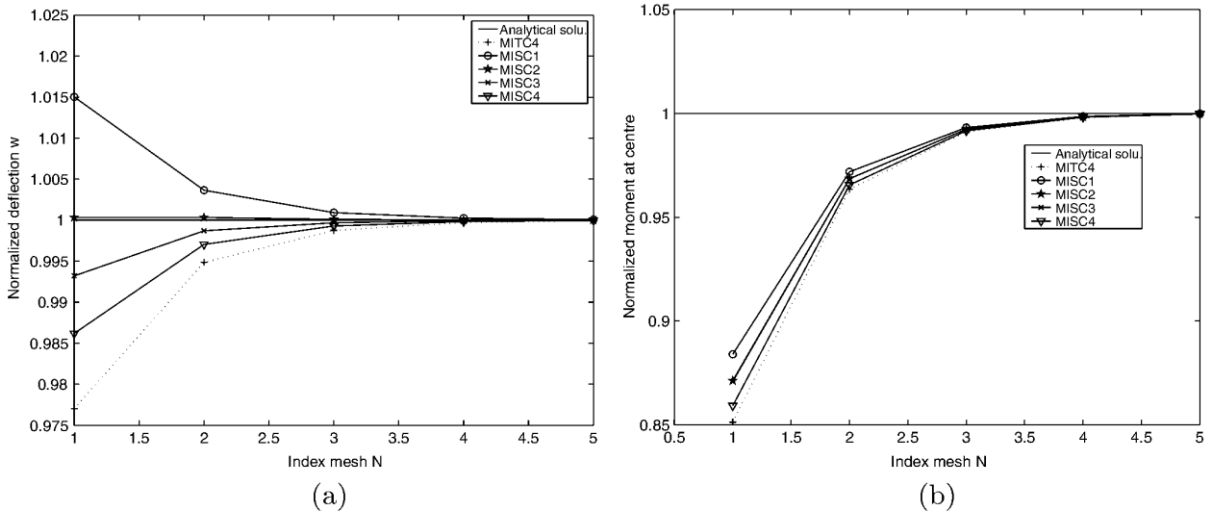

Figure 16. *Rate of convergence in energy norm for simply supported square plate subjected to uniform load.*

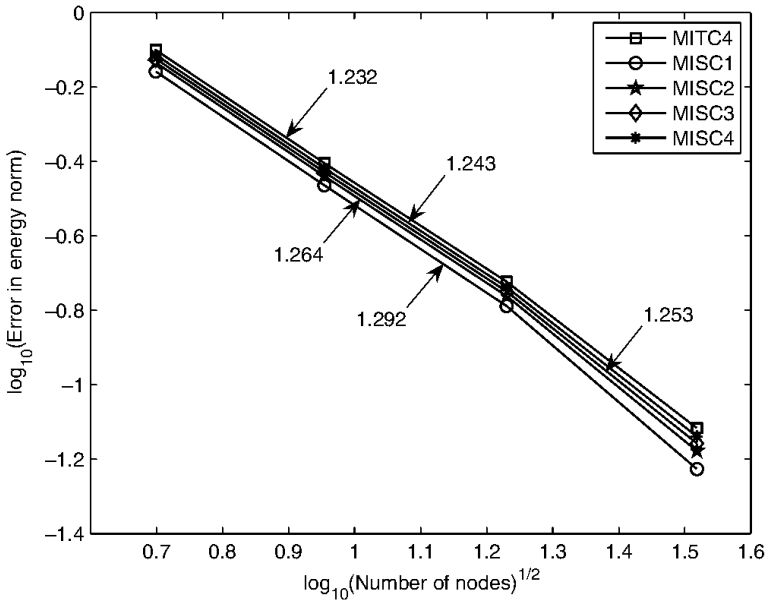

Published in : Computer methods in applied mechanics and engineering (2008), vol. 197, pp. 1184-1203
DOI: doi:10.1016/j.cma.2007.10.008
Status : Postprint (Author's version)

Figure 17. *A simply supported skew plate subjected to a uniform load.*

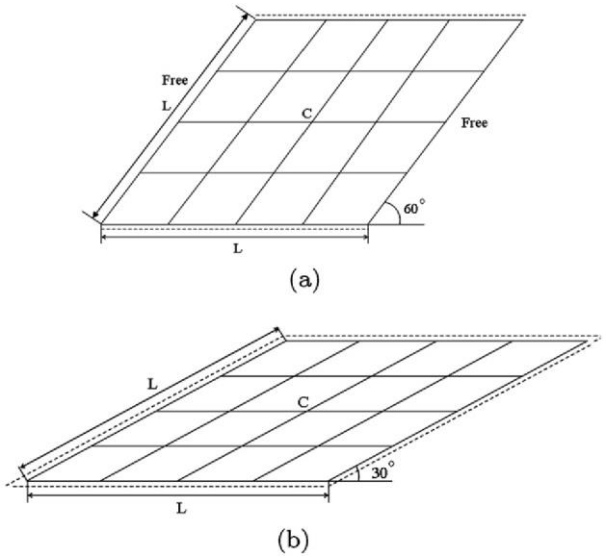

Figure 18. *A distribution of von Mises stress and level lines for Razzaque's skew plate using MISC4 element.*

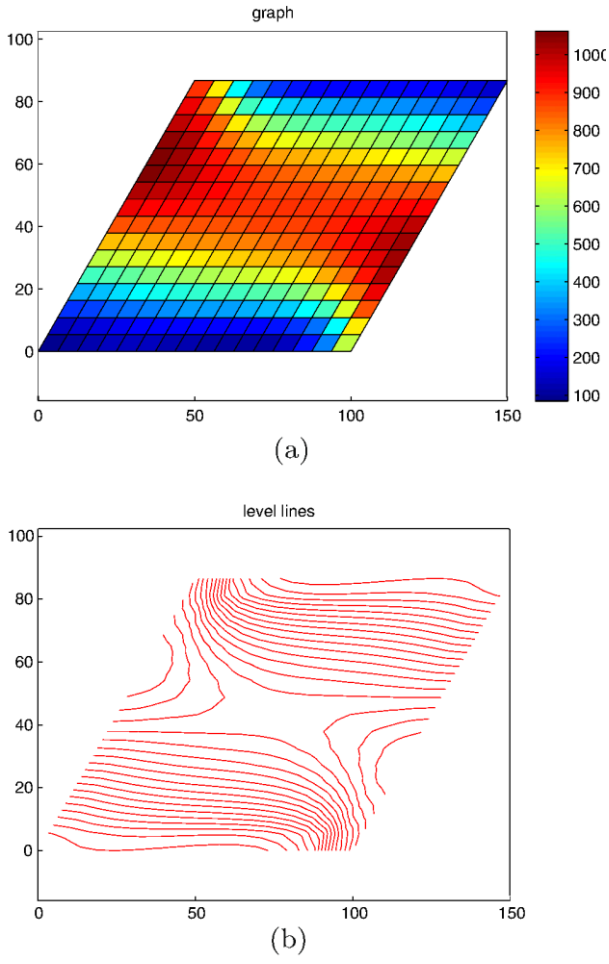

Published in : Computer methods in applied mechanics and engineering (2008), vol. 197, pp. 1184-1203
DOI: doi:10.1016/j.cma.2007.10.008
Status : Postprint (Author's version)

Figure 19. *A distribution of von Mises and level lines for Morley's skew plate using MISC2 element.*

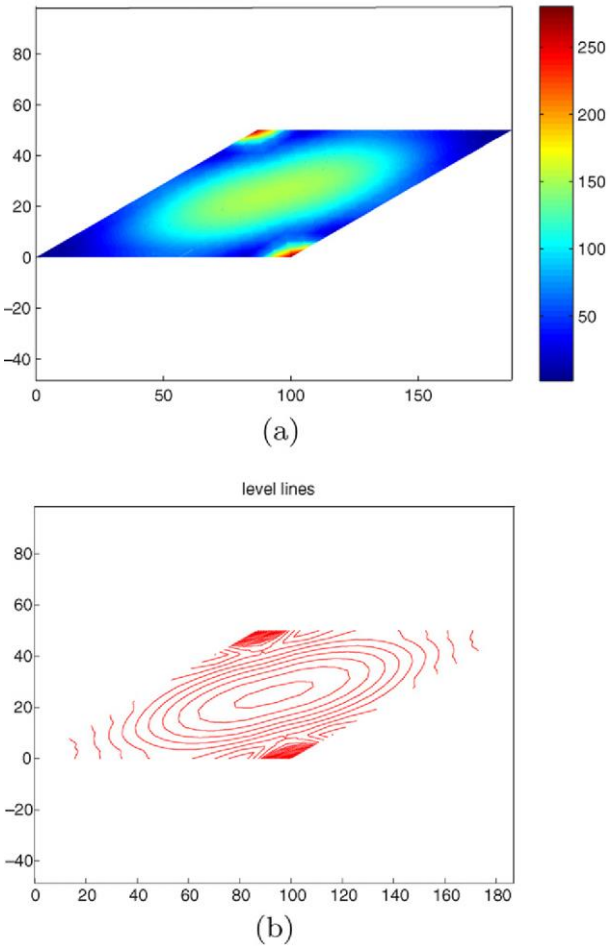

Published in : Computer methods in applied mechanics and engineering (2008), vol. 197, pp. 1184-1203
DOI: doi:10.1016/j.cma.2007.10.008
Status : Postprint (Author's version)

Figure 20. *The convergence of the central deflection w_c for Morley plate with different thickness/span ratio.*

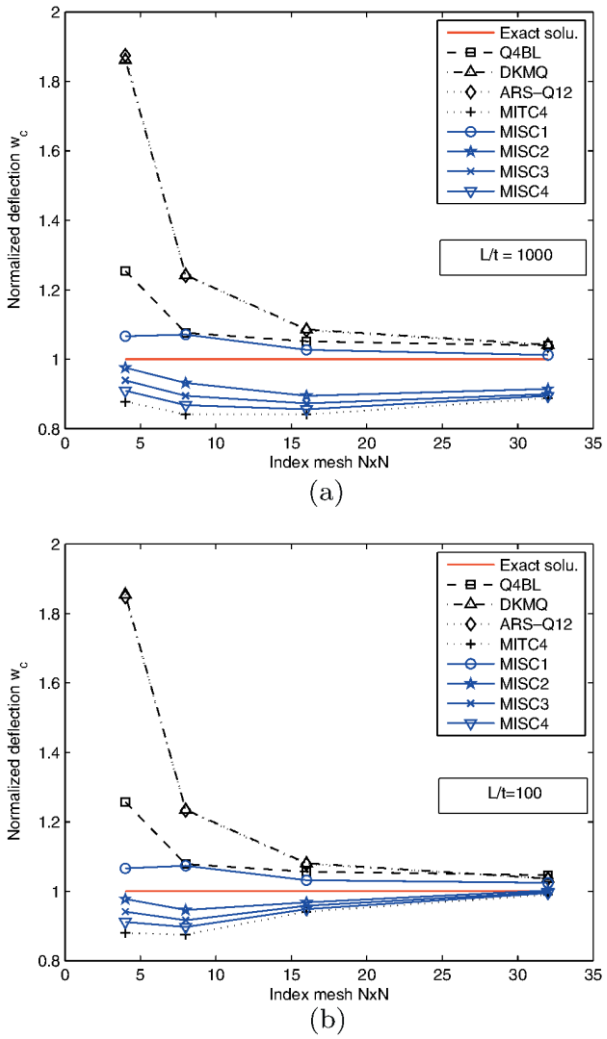

Figure 21. *Corner supported plate subjected to uniform load.*

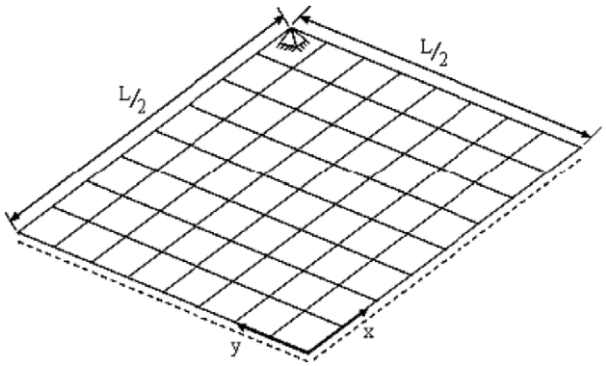

Published in : Computer methods in applied mechanics and engineering (2008), vol. 197, pp. 1184-1203
DOI: doi:10.1016/j.cma.2007.10.008
Status : Postprint (Author's version)

Figure 22. *Clamped circular plate subjected to concentrated load.*

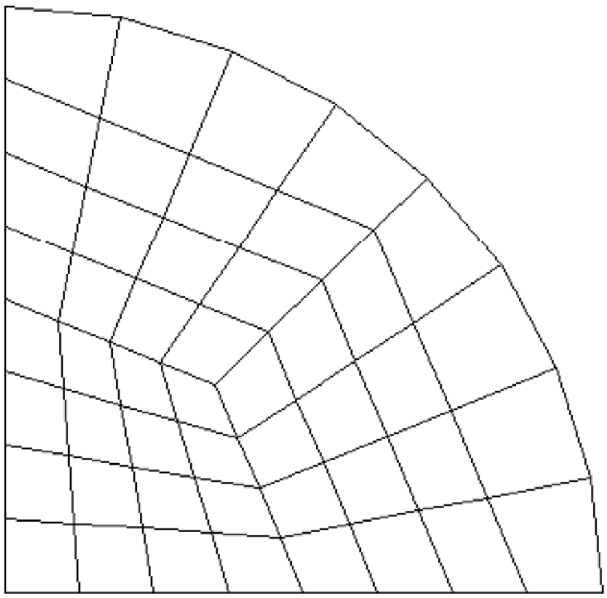

Figure 23. *Clamped circular plate subjected to concentrated load.*

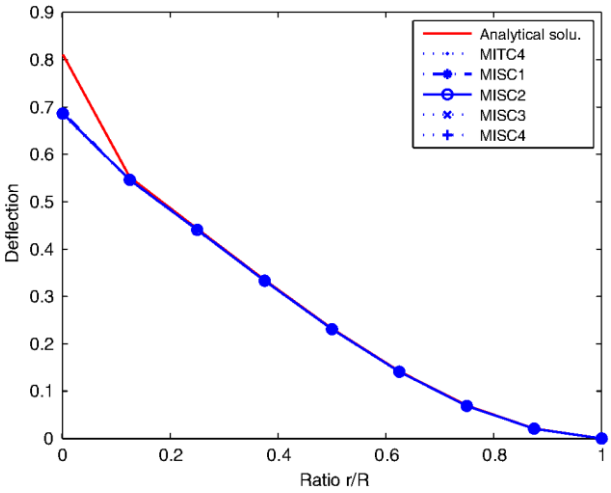

Published in : Computer methods in applied mechanics and engineering (2008), vol. 197, pp. 1184-1203
DOI: doi:10.1016/j.cma.2007.10.008
Status : Postprint (Author's version)

Table 1. *Patch test*

Element	W_5	Θ_{x5}	Θ_{y5}	m_{x5}	m_{y5}	m_{xy5}
Q4-R	0.5440	1.0358	-0.676	-	-	-
SC1Q4	0.5431	1.0568	-0.7314	-	-	-
SC2Q4	0.5439	1.0404	-0.6767	-	-	-
SC3Q4	0.5440	1.0396	-0.6784	-	-	-
SC4Q4	0.5439	1.0390	-0.6804	-	-	-
MITC4	0.5414	1.04	-0.55	-0.01111	-0.01111	-0.00333
MISC1	0.5414	1.04	-0.55	-0.01111	-0.01111	-0.00333
MISC2	0.5414	1.04	-0.55	-0.01111	-0.01111	-0.00333
MISC3	0.5414	1.04	-0.55	-0.01111	-0.01111	-0.00333
MISC4	0.5414	1.04	-0.55	-0.01111	-0.01111	-0.00333
Exact	0.5414	1.04	-0.55	-0.01111	-0.01111	-0.00333

-, no constant moments.

Table 2. *The central deflection $w_c/(pL^4/100D)$, $D = Et^3/12(1 - v^2)$ with mesh distortion for thin clamped plate subjected to uniform load p*

s	-1.249	-1.00	-0.5	0.00	0.5	1.00	1.249
CRB1 [59]	0.1381	0.1390	0.1247	0.1212	0.1347	0.1347	0.1249
CRB2 [59]	0.2423	0.1935	0.1284	0.1212	0.1331	0.1647	0.1947
S1 [59]	0.1105	0.1160	0.1209	0.1211	0.1165	0.1059	0.0975
S4R [1]	0.1337	0.1369	0.1354	0.1295	0.1234	0.1192	0.1180
DKQ [33]	0.1694	0.1658	0.1543	0.1460	0.1418	0.1427	0.1398
ANS-EC [32]	-	-	-	0.1303	-	-	-
ANS-2ND [32]	-	-	-	0.1240	-	-	-
Q4BL [65]	-	-	-	0.1113	-	-	-
NCQ [42]	-	-	-	0.1278	-	-	-
MITC4	0.0973	0.1032	0.1133	0.1211	0.1245	0.1189	0.1087
MISC1	0.1187	0.1198	0.1241	0.1302	0.1361	0.1377	0.1347
MISC2	0.1151	0.1164	0.1207	0.1266	0.1323	0.1331	0.1287
MISC3	0.1126	0.1144	0.1189	0.1249	0.1305	0.1309	0.1260
MISC4	0.1113	0.1130	0.1174	0.1233	0.1287	0.1288	0.1227
Exact solution	0.1265	0.1265	0.1265	0.1265	0.1265	0.1265	0.1265

Published in : Computer methods in applied mechanics and engineering (2008), vol. 197, pp. 1184-1203
DOI: doi:10.1016/j.cma.2007.10.008
Status : Postprint (Author's version)

Table 3. *Central deflections $w_c(pL^4/100D)$ for the clamped plate subjected to uniform load*

L/t	Elements	Mesh					Exact
		2	4	8	16	32	
10	MITC4	0.1431	0.1488	0.1500	0.1504	0.1504	0.1499
	MISC1	0.1517	0.1507	0.1505	0.1505	0.1505	
	MISC2	0.1483	0.1500	0.1503	0.1504	0.1505	
	MISC3	0.1467	0.1496	0.1502	0.1504	0.1504	
	MISC4	0.1451	0.1493	0.1502	0.1504	0.1504	
10^2	MITC4	0.1213	0.1253	0.1264	0.1267	0.1268	0.1267
	MISC1	0.1304	0.1274	0.1269	0.1268	0.1268	
	MISC2	0.1269	0.1266	0.1267	0.1268	0.1268	
	MISC3	0.1252	0.1262	0.1266	0.1267	0.1268	
	MISC4	0.1235	0.1258	0.1265	0.1267	0.1268	
10^3	MITC4	0.1211	0.1251	0.1262	0.1264	0.1265	0.1265
	MISC1	0.1302	0.1272	0.1267	0.1266	0.1265	
	MISC2	0.1266	0.1264	0.1265	0.1265	0.1265	
	MISC3	0.1249	0.1260	0.1264	0.1265	0.1265	
	MISC4	0.1233	0.1256	0.1263	0.1265	0.1265	
10^4	MITC4	0.1211	0.1251	0.1262	0.1264	0.1265	0.1265
	MISC1	0.1302	0.1272	0.1267	0.1266	0.1265	
	MISC2	0.1266	0.1264	0.1265	0.1265	0.1265	
	MISC3	0.1249	0.1260	0.1264	0.1265	0.1265	
	MISC4	0.1233	0.1256	0.1263	0.1265	0.1265	
105	MITC4	0.1211	0.1251	0.1262	0.1264	0.1265	0.1265
	MISC1	0.1302	0.1272	0.1267	0.1266	0.1265	
	MISC2	0.1266	0.1264	0.1265	0.1265	0.1265	
	MISC3	0.1249	0.1260	0.1264	0.1265	0.1265	
	MISC4	0.1233	0.1256	0.1263	0.1265	0.1265	

Table 4. *Central moments $M_c(pL^2/10)$ for the clamped plate subjected to uniform load*

L/t	Elements	Mesh					Exact
		2	4	8	16	32	
10	MITC4	0.1898	0.2219	0.2295	0.2314	0.2318	0.231
	MISC1	0.2031	0.2254	0.2304	0.2316	0.2319	
	MISC2	0.1982	0.2241	0.2300	0.2315	0.2319	
	MISC3	0.1974	0.2239	0.2300	0.2315	0.2319	
	MISC4	0.1930	0.2228	0.2297	0.2314	0.2319	
10^2	MITC4	0.1890	0.2196	0.2267	0.2285	0.2289	0.2291
	MISC1	0.2031	0.2233	0.2277	0.2287	0.2290	
	MISC2	0.1976	0.2218	0.2273	0.2286	0.2290	
	MISC3	0.1974	0.2217	0.2273	0.2286	0.2290	
	MISC4	0.1923	0.2205	0.2270	0.2286	0.2290	
10^3	MITC4	0.1890	0.2196	0.2267	0.2285	0.2289	0.2291
	MISC1	0.2031	0.2233	0.2276	0.2287	0.2290	
	MISC2	0.1976	0.2218	0.2273	0.2286	0.2289	
	MISC3	0.1974	0.2217	0.2272	0.2286	0.2289	
	MISC4	0.1923	0.2205	0.2269	0.2285	0.2289	
10^4	MITC4	0.1890	0.2196	0.2267	0.2285	0.2289	0.2291
	MISC1	0.2031	0.2233	0.2276	0.2287	0.2290	
	MISC2	0.1976	0.2218	0.2273	0.2286	0.2289	
	MISC3	0.1974	0.2217	0.2272	0.2286	0.2289	
	MISC4	0.1923	0.2205	0.2269	0.2285	0.2289	
10^5	MITC4	0.1890	0.2196	0.2267	0.2285	0.2289	0.2291
	MISC1	0.2031	0.2233	0.2276	0.2287	0.2290	
	MISC2	0.1976	0.2218	0.2273	0.2286	0.2289	
	MISC3	0.1974	0.2217	0.2272	0.2286	0.2289	
	MISC4	0.1923	0.2205	0.2269	0.2285	0.2289	

Published in : Computer methods in applied mechanics and engineering (2008), vol. 197, pp. 1184-1203
DOI: doi:10.1016/j.cma.2007.10.008
Status : Postprint (Author's version)

Table 5. *Central deflections $w_c/(pL^4/100D)$ for the simply supported plate subjected to uniform load*

L/t	Elements	Mesh					Exact [55]
		2	4	8	16	32	
10	MITC4	0.4190	0.4255	0.4268	0.4272	0.4273	0.4273
	MISC1	0.4344	0.4290	0.4277	0.4274	0.4273	
	MISC2	0.4285	0.4277	0.4274	0.4273	0.4273	
	MISC3	0.4256	0.4270	0.4272	0.4273	0.4273	
	MISC4	0.4227	0.4263	0.4271	0.4272	0.4273	
102	MITC4	0.3971	0.4044	0.4059	0.4063	0.4064	0.4064
	MISC1	0.4125	0.4079	0.4068	0.4065	0.4065	
	MISC2	0.4066	0.4066	0.4065	0.4065	0.4064	
	MISC3	0.4037	0.4059	0.4063	0.4064	0.4064	
	MISC4	0.4008	0.4052	0.4062	0.4064	0.4064	
103	MITC4	0.3969	0.4041	0.4057	0.4061	0.4062	0.4062
	MISC1	0.4123	0.4077	0.4066	0.4063	0.4063	
	MISC2	0.4064	0.4064	0.4063	0.4062	0.4062	
	MISC3	0.4035	0.4057	0.4061	0.4062	0.4062	
	MISC4	0.4006	0.4050	0.4059	0.4062	0.4062	
104	MITC4	0.3969	0.4041	0.4057	0.4061	0.4062	0.4062
	MISC1	0.4123	0.4077	0.4066	0.4063	0.4063	
	MISC2	0.4064	0.4064	0.4063	0.4062	0.4062	
	MISC3	0.4035	0.4057	0.4061	0.4062	0.4062	
	MISC4	0.4006	0.4050	0.4059	0.4062	0.4062	
105	MITC4	0.3969	0.4041	0.4057	0.4061	0.4062	0.4062
	MISC1	0.4123	0.4077	0.4066	0.4063	0.4063	
	MISC2	0.4064	0.4064	0.4063	0.4062	0.4062	
	MISC3	0.4035	0.4057	0.4061	0.4062	0.4062	
	MISC4	0.4006	0.4050	0.4059	0.4062	0.4062	

Published in : Computer methods in applied mechanics and engineering (2008), vol. 197, pp. 1184-1203
DOI: doi:10.1016/j.cma.2007.10.008
Status : Postprint (Author's version)

Table 6. *Central moments $M_c/(pL^2/10)$ for the simply supported plate subjected to uniform load.*

L/t	Elements	Mesh					Exact [55]
		2	4	8	16	32	
10	MITC4	0.4075	0.4612	0.4745	0.4778	0.4786	
	MISC1	0.4232	0.4652	0.4755	0.4780	0.4787	
	MISC2	0.4172	0.4637	0.4751	0.4779	0.4786	
	MISC3	0.4169	0.4637	0.4751	0.4779	0.4786	
	MISC4	0.4113	0.4622	0.4747	0.4778	0.4786	
10^2	MITC4	0.4075	0.4612	0.4745	0.4778	0.4786	
	MISC1	0.4232	0.4652	0.4755	0.4780	0.4787	
	MISC2	0.4171	0.4637	0.4751	0.4779	0.4786	
	MISC3	0.4169	0.4636	0.4751	0.4779	0.4786	
	MISC4	0.4113	0.4622	0.4747	0.4778	0.4786	0.4789
103	MITC4	0.4075	0.4612	0.4745	0.4778	0.4786	
	MISC1	0.4232	0.4652	0.4755	0.4780	0.4787	
	MISC2	0.4171	0.4637	0.4751	0.4779	0.4786	
	MISC3	0.4169	0.4636	0.4751	0.4779	0.4786	
	MISC4	0.4113	0.4622	0.4747	0.4778	0.4786	
10^4	MITC4	0.4075	0.4612	0.4745	0.4778	0.4786	
	MISC1	0.4232	0.4652	0.4755	0.4780	0.4787	
	MISC2	0.4171	0.4637	0.4751	0.4779	0.4786	
	MISC3	0.4169	0.4636	0.4751	0.4779	0.4786	
	MISC4	0.4113	0.4622	0.4747	0.4778	0.4786	
10^5	MITC4	0.4075	0.4612	0.4745	0.4778	0.4786	
	MISC1	0.4232	0.4652	0.4755	0.4780	0.4786	
	MISC2	0.4171	0.4637	0.4751	0.4779	0.4786	
	MISC3	0.4169	0.4636	0.4751	0.4779	0.4786	
	MISC4	0.4113	0.4622	0.4747	0.4778	0.4786	

Table 7. *Central defection and moment of the Razzaque's skew plate*

Mesh	MITC4	MISC1	MISC2	MISC3	MISC4
(a) Central defection $w_c/10^4$					
2 x 2	0.3856	0.3648	0.3741	0.3781	0.3816
4 x 4	0.6723	0.6702	0.6725	0.6725	0.6724
6 x 6	0.7357	0.7377	0.7377	0.7370	0.7364
8 x 8	0.7592	0.7615	0.7610	0.7604	0.7598
12 x 12	0.7765	0.7781	0.7776	0.7772	0.7769
16 x 16	0.7827	0.7838	0.7834	0.7832	0.7830
32 x 32	0.7888	0.7892	0.7891	0.7890	0.7889
Ref. [51,6]					0.7945
(b) Central moment $M_y/10^3$					
2 x 2	0.4688	0.4688	0.4688	0.4688	0.4688
4 x 4	0.8256	0.8321	0.8301	0.8284	0.8269
6 x 6	0.8976	0.9020	0.9005	0.8994	0.8984
8 x 8	0.9242	0.9272	0.9260	0.9254	0.9245
12 x 12	0.9439	0.9454	0.9448	0.9445	0.9442
16 x 16	0.9510	0.9518	0.9515	0.9513	0.9511
32 x 32	0.9577	0.9580	0.9579	0.9578	0.9578
Ref. [51,6]					0.9589

Published in : Computer methods in applied mechanics and engineering (2008), vol. 197, pp. 1184-1203
DOI: doi:10.1016/j.cma.2007.10.008
Status : Postprint (Author's version)

Table 8. *The convergence of center defection for corner supported plate.*

Elem. per side	8	16	24	48	96
DKQ [33]	0.11914	0.11960	0.11969	0.11974	0.11975
G/W [27]	0.11862	0.11947	0.11963	0.11973	0.11975
MITC4	0.11856	0.11946	0.11963	0.11973	0.11975
MISC1	0.11873	0.11950	0.11965	0.11973	0.11975
MISC2	0.11867	0.11949	0.11964	0.11973	0.11975
MISC3	0.11864	0.11948	0.11963	0.11973	0.11975
MISC4	0.11861	0.11947	0.11963	0.11973	0.11975
Theory					0.12253

Table 9. *Three lowest frequencies for corner supported plate.*

Element	6 x 6 mesh			32 x 32 mesh		
	$\bar{\omega}_1$	$\bar{\omega}_2$	$\bar{\omega}_3$	$\bar{\omega}_1$	$\bar{\omega}_2$	$\bar{\omega}_3$
DKQ [33]	7.117	18.750	43.998	-	-	-
G/W [27]	7.144	18.800	44.105	-	-	-
MITC4	7.135	18.795	44.010	7.03	18.652	43.16
MISC1	7.136	18.799	44.011	7.07	18.661	43.55
MISC2	7.141	18.800	44.065	7.07	18.661	43.55
MISC3	7.143	18.800	44.092	7.07	18.661	43.55
MISC4	7.145	18.800	44.119	7.07	18.661	43.55
Theory [38]				7.12	19.600	44.40

Table 10. *The normalized defection at center for circular plate.*

Mesh	2	4	8	16	32
MITC4	0.7817	0.8427	0.8874	0.9278	0.9671
MISC1	0.8011	0.8492	0.8893	0.9284	0.9673
MISC2	0.7910	0.8457	0.8883	0.9281	0.9672
MISC3	0.7880	0.8448	0.8880	0.9280	0.9672
MISC4	0.7854	0.8439	0.8877	0.9279	0.9672

Published in : Computer methods in applied mechanics and engineering (2008), vol. 197, pp. 1184-1203
DOI: doi:10.1016/j.cma.2007.10.008
Status : Postprint (Author's version)

References

[1] ABAQUS/Standard User's Manual, Version 6.4, Hibbitt, Karlsson and Sorensen, Inc., Rawtucket, Rhode Island, 2004.

[2] F. Armero, D. Ehrlich, Finite element methods for the multi-scale modeling of softening hinge lines in plates at failure.

[3] K.J. Bathe, Finite Element Procedures, Prentice-Hall/MIT, Englewood Cliffs, NJ/MA, 1996.

[4] K.J. Bathe, E.N. Dvorkin, A four-node plate bending element based on Mindlin/Reissener plate theory and a mixed interpolation, Int. J. Numer. Methods Engrg. 21 (1985) 367-383.

[5] K.J. Bathe, E.N. Dvorkin, A formulation of general shell elements. the use of mixed interpolation of tensorial components, Int. J. Numer. Methods Engrg. 22 (1986) 697-722.

[6] J.L. Batoz, G. Dhatt, Modelisation des structures par elements finis, vol. 2, poutres et plaques, Hermes, 1990.

[7] G.P. Bazeley, Y.K. Cheung, B.M. Irons, O.C. Zienkiewicz, Triangular Elements in Plate Bending, Proceedings of the First Conference, on Matrix Methods in Structural Mechanics, Wright-Patterson AFB, Ohio, 1965.

[8] T. Belytschko, T. Black, Elastic crack growth in finite elements with minimal remeshing, Int. J. Numer. Methods Engrg. 45 (5) (1999) 601620.

[9] T. Belytschko, N. Moes, S. Usui, C. Parimi, Arbitrary discontinuities in finite elements, Int. J. Numer. Methods Engrg. 50 (4) (2001) 9931013.

[10] K. Bletzinger, M. Bischoff, E. Ramm, A unified approach for shearlocking-free triangular and rectangular shell finite elements, Comput. Struct. 75 (2000) 321-334.

[11] S. Bordas, J.G. Conley, B. Moran, J. Gray, E. Nichols, A simulationbased design paradigm for complex cast components, Engrg. Com- put. 23 (1) (2007) 25-37.

[12] S. Bordas, M. Duflot, Derivative recovery and a posteriori error estimation in extended finite element methods, Comput. Methods Appl. Mech. Engrg., in press, http://dx.doi.org/10.1016/ j.cma.2007.03.011.

[13] S. Bordas, M. Duflot, P. Le, A simple a posteriori error estimator for the extended finite element method, Commun. Numer. Methods Engrg., in press, doi:10.1002/cnm.1001.

[14] S. Bordas, B. Moran, Enriched finite elements and level sets for damage tolerance assessment of complex structures, Engrg. Fract. Mech. 73 (2006) 1176-1201.

[15] S. Bordas, V.P. Nguyen, C. Dunant, H. Nguyen-Dang, A. Guid- oumm, An extended finite element library, Int. J. Numer. Methods Engrg., doi:10.1002/nme.1966.

[16] S. Bordas, T. Rabczuk, G. Zi, Three-dimensional crack initiation, propagation, branching and junction in non-linear materials by an extended meshfree method without asymptotic enrichment, Engrg. Fract. Mech., in press, doi:10.1016/j.engfracmech.2007.05.010.

[17] J.S. Chen, C.T. Wu, S. Yoon, Y. You, A stabilized conforming nodal integration for Galerkin mesh-free methods, Int. J. Numer. Methods Engrg. 50 (2001) 435-466.

Published in : Computer methods in applied mechanics and engineering (2008), vol. 197, pp. 1184-1203
DOI: doi:10.1016/j.cma.2007.10.008
Status : Postprint (Author's version)

[18] W. Chen, Y.K. Cheung, Refined quadrilateral element based on Mindlin/Reissner plate theory, Int. J. Numer. Methods Engrg. 47 (2000) 605-627.

[19] C. Chinosi, C. Lovadina, L.D. Marini, Nonconforming locking-free finite elements for Reissner-Mindlin plates, Comput. Methods Appl. Mech. Engrg. 195 (2006) 3448-3460.

[20] K.Y. Dai, G.R. Liu, Free and forced vibration analysis using the smoothed finite element method (SFEM), J. Sound Vibration 301 (35) (2007) 803-820.

[21] K.Y. Dai, G.R. Liu, T.T. Nguyen, An n-sided polygonal smoothed finite element method (nSFEM) for solid mechanics, Finite Elements Anal. Design 43 (11-12) (2007) 847-860.

[22] M. Duflot, S. Bordas, An extended global recovery procedure for a posteriori error estimation in extended finite element methods, Int. J. Numer. Methods Engrg., in press.

[23] C. Dunant, P. Nguyen, M. Belgasmia, S. Bordas, A. Guidoum, H. Nguyen-Dang, Architecture trade-offs of including a mesher in an object-oriented extended finite element code, Eur. J. Mech. (16) (2007) 237-258 (special issue on the extended finite element method).

[24] E.N. Dvorkin, K.J. Bathe, A continuum mechanics based four-node shell element for general nonlinear analysis, Engrg. Comput. (1994).

[25] B. Fraeijs de Veubeke, G. Sander, An equilibrium model for plate bending, International Journal of Solids Structures, Pergamon Press, London, 1968.

[26] O. Garcia, E.A. Fancello, C.S. Barcellos, C.A. Duarte, *Hp* clouds in Mindlin's thick plate model, Int. J. Numer. Methods Engrg. 47 (2000) 1381-1400.

[27] F. Gruttmann, W. Wagner, A stabilized one-point integrated quadrilateral Reissener-Mindlin plate element, Int. J. Numer. Methods Engrg. 61 (2004) 2273-2295.

[28] T.J.R. Hughes, The Finite Element Method, Prentice-Hall, Englewood Cliffs, NJ, 1987.

[29] T.J.R. Hughes, M. Cohen, M. Haroun, Reduced and selective integration techniques in finite element method of plates, Nuclear Engrg. Des. 46 (1978) 203-222.

[30] T.J.R. Hughes, R.L. Taylor, W. Kanoknukulchai, Simple and efficient element for plate bending, Int. J. Numer. Methods Engrg. 11 (1977) 1529-1543.

[31] T.J.R. Hughes, T. Tezduyar, Finite elements based upon Mindlin plate theory with particular reference to the four-node isoparametric element, J. Appl. Mech. (1981).

[32] D.D. Jensen, K.C. Park, Equilibrium constrained assumed natural co-ordinate strain plate elements, Int. J. Numer. Methods Engrg. 38 (1995) 2951-2977.

[33] J.L. Batoz, M.B. Tahar, Evaluation of a new quadrilateral thin plate bending element, Int. J. Numer. Methods Engrg. 18 (1982) 16551677.

[34] P. Krysl, T. Belytschko, Analysis of thin plates by the element-free Galerkin method, Comput. Mech. 16 (1995) 1-10.

[35] P. Krysl, T. Belytschko, Analysis of thin shells by the element-free Galerkin method, Int. J. Numer. Methods Engrg. 33 (1996) 30573080.

[36] S.W. Lee, T.H.H. Pian, Improvement of plate and shell finite element by mixed formulation, AIAA J. 16 (1978) 29-34.

Published in : Computer methods in applied mechanics and engineering (2008), vol. 197, pp. 1184-1203
DOI: doi:10.1016/j.cma.2007.10.008
Status : Postprint (Author's version)

[37] S.W. Lee, C. Wong, Mixed formulation finite elements for Mindlin theory plate bending, Int. J. Numer. Methods Engrg. 18 (1982) 12971311.

[38] A.W. Leissa, Vibration of plates, NASA SP-160 (1969).

[39] Q. Li, J. Soric, T. Jarak, S.N. Atluri, A locking-free meshless local Petrov-Galerkin formulation for thick and thin plates, J. Comput. Phys. 208 (2005) 116-133.

[40] G.R. Liu, K.Y. Dai, T.T. Nguyen, A smoothed finite element for mechanics problems, Comput. Mech. 39 (2007) 859-877.

[41] G.R. Liu, T.T. Nguyen, K.Y. Dai, K.Y. Lam, Theoretical aspects of the smoothed finite element method (SFEM), Int. J. Numer. Methods Engrg. 71 (8) (2007) 902-930.

[42] I.W. Liu, C.C. Lin, A new conforming quadrilateral plate bending element, Int. J. Numer. Methods Engrg. 36 (1993) 2921-2937.

[43] N. Moes, T. Belytschko, Extended finite element method for cohesive crack growth, Engrg. Fract. Mech. 69 (2002) 813-834.

[44] N. Moes, J. Dolbow, T. Belytschko, A finite element method for crack growth without remeshing, Int. J. Numer. Methods Engrg. 46 (1)(1999) 133-150.

[45] L.S.D. Morley, Skew Plates and Structures, Pergamon Press, Oxford, 1963.

[46] X.H. Nguyen, S. Bordas, H. Nguyen-Dang, Smooth strain finite elements: selective integration. Collection of Papers from Prof. Nguyen-Dang Hung's former students, Vietnam National University, HCM Publishing House, 2006, pp. 88-106.

[47] T.T. Nguyen, G.R. Liu, K.Y. Dai, K.Y. Lam, Selective smoothed finite element method, Tsinghua Sci. Tech. 12 (5) (2007) 497-508.

[48] T.H.H. Pian, P. Tong, Basis of finite elements for solids continua, Int. J. Numer. Methods Engrg. 1 (1969) 3-28.

[49] G. Prathap, The Finite Element Method in Structural Mechanics, Kluwer Academic Publishers, Dordrect, 1993.

[50] T. Rabczuk, S. Bordas, G. Zi, A three-dimensional meshfree method for continuous crack initiation, nucleation and propagation in statics and dynamics, Comput. Mech., 2007, doi:10.1007/s00466-006-0122-1.

[51] A. Razzaque, Program for triangular bending elements with derivative smoothing, Int. J. Numer. Methods Engrg. 6 (1973) 333-345.

[52] J.C. Simo, T.J.R. Hughes, On the variational foundation of assumed strain methods, ASME J. Appl. Mech. 53 (1986) 51-54.

[53] J.C. Simo, M.S. Rifai, A class of mixed assumed strain methods and the method of incompatible modes, Int. J. Numer. Methods Engrg. 29 (1990) 1595-1638.

[54] J. Soric, Q. Li, T. Jarak, S.N. Atluri, The meshless local Petrov- Galerkin (MLPG) formulation for analysis of thick plates, Comput. Model. Engrg. Sci. 6 (2004) 349-357.

[55] R.L. Taylor, F. Auricchio, Linked interpolation for Reissner-Mindlin plate elements. Part I - A simple triangle, Int. J. Numer. Methods Engrg. 36 (1993) 3056-3066.

Published in : Computer methods in applied mechanics and engineering (2008), vol. 197, pp. 1184-1203
DOI: doi:10.1016/j.cma.2007.10.008
Status : Postprint (Author's version)

[56] D. Wang, J.S. Chen, Locking-free stabilized conforming nodal integration for meshfree Mindlin-Reissner plate formulation, Comput. Methods Appl. Mech. Engrg. 193 (2004) 1065-1083.

[57] D. Wang, S.B. Dong, J.S. Chen, Extended meshfree analysis of transverse and inplane loading of a laminated anisotropic plate of general planform geometry, Int. J. Solids Struct. 43 (2006) 144-171.

[58] K. Washizu, Variational Methods in Elasticity and Plasticity, third ed., Pergamon Press, New York, 1982.

[59] S.L. Weissman, R.L. Taylor, Resultant fields for mixed plate bending elements, Comput. Methods Appl. Mech. Engrg. 79 (1990) 321-355.

[60] E. Wyart, Three-dimensional crack analysis in aeronautical structures using the Substructured Finite Element/Extended Finite Element Method, PhD thesis, Universite catholique de Louvain, 2007.

[61] E. Wyart, D. Coulon, M. Duflot, T. Pardoen, J.-F. Remacle, F. Lani, A substructured fe shell/xfe 3d method for crack analysis. Int. J. Numer. Methods Engrg., in press.

[62] E. Wyart, D. Coulon, P. Martiny, T. Pardoen, J.-F. Remacle, F. Lani, A substructured fe/xfe method for stress intensity factors computation in an industrial structure, Rev. Eur. Mecanique Numerique, in press.

[63] E. Wyart, M. Duflot, D. Coulon, P. Martiny, T. Pardoen, J.-F. Remacle, F. Lani, Substructuring fe-xfe approaches applied to rack propagation, J. Comput. Appl. Math., in press.

[64] J.W. Yoo, B. Moran, J.S. Chen, Stabilized conforming nodal integration in the natural-element method, Int. J. Numer. Methods Engrg. 60 (2004) 861-890.

[65] O.C. Zienkiewicz, L.F. Zeng, Z. Xu, A. Samuelsson, N.E. Wiberg, Linked interpolation for Reissner-Mindlin plate elements: Part i-a simple quadrilateral, Int. J. Numer. Methods Engrg. 36 (1993) 30433056.

[66] O.C. Zienkiewicz, R.L. Taylor, The Finite Element Method, fifth ed., Butterworth-Heinemann, Oxford, 2000.

O.C. Zienkiewicz, R.L. Taylor, J.M. Too, Reduced integration technique in general analysis of plates and shells simple and efficient element for plate bending, Int. J. Numer. Methods Engrg. 3 (1971) 275-290